DEPARTMENT OF PHYSICS

NOVA SCHOOL OF SCIENCE & TECHNOLOGY

MAFALDA MIRANDA SALREU MARTINHO

BSc in Biomedical Engineering Sciences

A SOFT AND SMART TELEHEALTH SYSTEM

HAND REHABILITATION DEVICE FOR GRASPING FORCE ASSESSMENT OF POST STROKE PATIENTS

MASTER IN BIOMEDICAL ENGINEERING

NOVA University Lisbon

, September, 2023

NOVA SCHOOL OF
SCIENCE & TECHNOLOGY

DEPARTMENT OF PHYSICS

A SOFT AND SMART TELEHEALTH SYSTEM

HAND REHABILITATION DEVICE FOR GRASPING FORCE ASSESSMENT OF POST STROKE PATIENTS

MAFALDA MIRANDA SALREU MARTINHO

BSc in Biomedical Engineering Sciences

Adviser: Gursel Alici
Executive Dean, University of Wollongong

Co-adviser: Carla Maria Quintão Pereira
Auxiliar Professor, NOVA University Lisbon

Examination Committee

Chair: Name of the committee chairperson
Full Professor, FCT-NOVA

Rapporteur: Name of a rapporteur
Associate Professor, Another University

Members: Another member of the committee
Full Professor, Another University

Yet another member of the committee
Assistant Professor, Another University

MASTER IN BIOMEDICAL ENGINEERING

NOVA University Lisbon
, September, 2023

A Soft and Smart Telehealth System
Hand Rehabilitation Device for Grasping Force Assessment of Post Stroke Patients

This document was created with the (pdf/Xe/Lua)LaTeX processor and the NOVAthesis template (v7.0.3) [1].

To my beloved ones.

Acknowledgements

I would like to extend my heartfelt gratitude to all those who have contributed in any way to the realization of this project.

I want to extend a special and heartfelt thank you to my advisors, Professor Gursel Alici and co-advisor Dr. Hao Zhou, from the University of Wollongong. Their unwavering support, confidence, wealth of knowledge, and expert guidance not only equipped me with the resources and opportunities to excel in this project but also facilitated a significant period of learning and growth.

I am also deeply appreciative of my co-advisor, Dr. Carla Maria Quintão Pereira, from the NOVA School of Science and Technology, for her insightful conversations and practical suggestions that have greatly enriched this endeavor.

To the University of Wollongong, I extend my gratitude for accepting me during this period and for offering outstanding research facilities and support, which have fostered the flourishing of scientific knowledge.

A warm thank you goes out to all the wonderful individuals I had the pleasure of meeting during my time at UOW, Australia. Your camaraderie, encouragement, and the moments of joy we shared were instrumental in keeping my motivation high. Without your presence, this journey would have undoubtedly been more arduous. I would also like to express my thanks to the AMBER research group for the wealth of knowledge they shared.

To the NOVA School of Science and Technology, thank you for molding me into an engineer over the past five years, providing an environment of excellence, and boasting an exceptional campus.

Lastly, I appreciate the Physics Department for affording me the opportunity, delivering quality education, and fostering excellent relationships between teachers, researchers, and students.

To my parents, Cristina e Emanuel, thank you for always being there for me, for your patience, and to teach me how to be ambitious and pursue my dreams. Thank you for having had the patience to handle me and say no when I needed, and wishing or not, heling me to be even more strong and persistent with my dreams, fighting and never

quiting. I know the pivotal importance you had during my journey and that every lesson counted to where I reached today.

To my dear sister Joana, who, despite being my elder, never failed to tease me throughout my childhood, thank you for consistently being my pillar of strength. Your understanding, support, and pride in my achievements have been a driving force. Your tenacity and resilience have inspired me to reach for greater heights and embrace challenges. Additionally, I appreciate the invaluable academic advice you've provided.

To my grandparents, who may have viewed my multitasking tendencies as a touch of madness, I want to express how crucial your love and support have been in maintaining my demanding schedule. To my grandmothers, who nourished me like royalty and even assisted with my laundry, I've come to realize the unmatched comfort of our cherished home after relocating to Australia.

To my partner, João, who has unwaveringly supported me through every challenge, willingly molding his life to bring my dreams to life, ultimately guiding me to become the finest version of myself.

To my loyal companion, Maré, whose exceptional listening skills and delightful presence brought boundless joy. Making you happy was always a source of immense fulfillment.

To my cherished friends, who lent an ear, offered sage advice, and shared in the same struggles during this phase of life, I want to extend my deepest thanks. You have consistently uplifted my spirits, filling my days with joy and imbuing them with a sense of vitality through our shared adventures.

To my Kickboxing coach, Vidal, and the entire team, without whom I could never have achieved the athletic milestones I reached. Your unyielding determination, passion, belief, and encouragement were the cornerstones of my success.

To each and every one of you, thank you from the bottom of my heart!

”

“It’s supposed to be hard. If it were easy, everyone would do it.”

— Tom Hanks, en

Abstract

The assessment of post-stroke patient rehabilitation currently lacks a comprehensive approach, often relying on subjective evaluations without a universally accepted quantitative method. In this study, a sensorised device was developed to contribute to bridging this gap. This device interfaces with a platform enabling therapists to visually analyse real-time data and facilitates data retrieval for in-depth analysis.

This research involved the creation and characterisation of several pneumatic sensors using Finite Element Anaysis (FEA) and mechanical testing. After meticulous shape selection, multiple sensors were calibrated and integrated into a cylindrical object. Communication was established through two multiplexers and an Arduino Nano, resulting in a compact and portable object. This system was then connected to a laptop via USB, utilising a LabVIEW program as the user interface. This program enabled the concurrent measurement of individual finger forces during grasping movements for both hands. Real-time data visualization and subsequent data retrieval were also supported.

The system adeptly addresses the identified limitations, emerging as a cost-effective, precise, and adaptable tool. Subsequent improvements are expected to fine-tune its precision, durability, and relevance within stroke rehabilitation scenarios. In this regard, the innovative tool, which is the primary contribution of this study, holds the potential to substantially elevate rehabilitation strategies and play a pivotal role in augmenting the recovery process.

The research work described in this dissertation was carried out in accordance with the norms established in the ethics code of Universidade Nova de Lisboa. The work described and the material presented in this dissertation, with the exceptions clearly indicated, constitute original work carried out by the author

Keywords: Stroke, Hand rehabilitation, Sensorised objects, Grasping force, Flexible sensors, Hand Anatomy

Resumo

A avaliação da reabilitação de pacientes após Acidente Vascular Cerebral carece atualmente de uma abordagem abrangente, muitas vezes dependendo de avaliações subjetivas sem um método quantitativo universalmente aceite. Neste estudo, um dispositivo sensorizado foi desenvolvido para ajudar a colmatar esta lacuna. Este dispositivo interage com uma plataforma que permite aos terapeutas analisar visualmente dados em tempo real e facilita a recuperação de dados para análise detalhada.

Este projeto envolveu a criação e caracterização de vários sensores pneumáticos utilizando o método de Análise de Elementos Finitos bem como testes mecânicos. Após uma seleção meticulosa de formas, vários sensores foram calibrados e integrados num objeto cilíndrico. A comunicação foi estabelecida através de dois multiplexadores e um Arduino Nano, resultando num objeto compacto e portátil. Este sistema foi então ligado a um computador portátil via USB, utilizando um programa LabVIEW como interface com o utilizador. Este programa permitiu a medição simultânea das forças individuais dos dedos durante os movimentos de preensão palmar de ambas as mãos. A visualização de dados em tempo real e a subsequente recuperação de dados também foram suportadas.

O sistema aborda de forma hábil as limitações identificadas, emergindo como uma ferramenta eficaz, precisa e adaptável em termos de custos. Melhorias subsequentes têm como objetivo afinar a sua precisão, durabilidade e relevância em cenários de reabilitação. Neste sentido, esta ferramenta inovadora, que é o principal contributo deste estudo, tem o potencial de elevar substancialmente as estratégias de reabilitação correntes e desempenhar um papel fundamental no melhoramento do processo de recuperação.

O trabalho de investigação descrito nesta dissertação foi realizado de acordo com as normas estabelecidas no código de ética da Universidade Nova de Lisboa. O trabalho descrito e o material apresentado nesta dissertação, com as exceções claramente indicadas, constituem trabalho original realizado pela autora.

Palavras-chave: AVC, Rehabilitação da mão, Objetos sensorisados, Força de preensão palmar, Sensores flexíveis, Anatomia da mão

Contents

List of Figures

List of Tables

Glossary

Hemiplegia Muscular paralysis affecting a single side of the body, involving the lower face, arm, and leg *(p. 7)*

Spasticity Unusual surge in muscle tension or rigidity, potentially impeding motion, speech, or correlating with unease or discomfort. *(p. 8)*

Acronyms

CAD Computer-Aided Design *(pp. 14, 15, 20)*
CMC Carpometacarpal *(p. 6)*
CMSA Chedoke-McMaster Stroke Assessment *(p. 7)*

DALYs Disability adjusted life years *(p. 1)*
DIP Distal Interphalangeal *(pp. 6–8)*

FEA Finite Element Anaysis *(pp. vi, x, 15, 17, 21, 25, 32, 33)*
FEM Finite Element Modeling *(pp. x, xii, 16, 19–21, 24, 33)*
FFF Fused filament fabrication *(pp. 14, 25)*
FMA Fugl-Meyer Assessment *(pp. 7, 10)*
FSR Force Sensing Resistor *(pp. 8, 9)*

IMU Inertial measurement unit *(p. 9)*
IP Interphalangeal *(p. 6)*

MCP Metacarpophalangeal *(p. 6)*
MUX Multiplexers *(pp. 28, 29)*

NIHSS National Institutes of Health Stroke Scale *(p. 7)*

PIP Proximal Interphalangeal *(p. 6)*
PSC Pneumatic Sensing Chamber *(pp. x, xi, 2, 11–13, 16–18, 21–29, 32, 33)*

ROM Range of Motion *(pp. 2, 7, 8)*

TPU Thermoplastic polyurethane *(pp. 14, 15)*

UTM Universal Testing Machine *(pp. x, 16–18, 20, 21, 23)*

1

Introduction

1.1 Objectives and Motivation

According with Global Burden of Diseases, Injuries, and Risk Factors Study (GBD 2010) [2], stroke was the second leading cause of death and the third leading cause of Disability adjusted life years (DALYs) worldwide in 2010 [3]. Stroke survivors often experience severe health constrains, with motor impairments being a common consequence that can lead to functional limitations in daily activities, causing long term consequences for patients and their families [4]. The burden of stroke survivors on society as a whole is significant and constantly growing [5], with studies projecting a global increase of 200 million DALYs lost due to stroke by 2030 [5]. Roughly 50 % of post stroke survivors experience upper limb impairment [6].

Hand rehabilitation is a crucial aspect of post-stroke recovery, as the ability to use one's hands impacts the performance of basic activities of daily living, as well as social participation and quality of life [7]. Conventional hand rehabilitation for stroke patients often involves repetitive exercises and physical therapy, which can be time-consuming, costly, and limited in individualized feedback [8].

Considering the rising incidence of stroke and the significant loss of DALYs due to stroke, along with the already burdened healthcare resources worldwide and the constraints highlighted by the COVID-19 pandemic, telehealth systems are an increasing solution for the future of healthcare [9], [10]. These services should incorporate self-directed rehabilitation strategies, making them accessible in both community and home-based therapy settings [10]. Moreover, to enrich neurorehabilitation and improve stroke outcome in general, understanding the underlying recovery route must be address since observational analysis on itself is not sufficient to measure the patient's improvement. [11].

Recent advancements in sensor technology have enabled the development of telemonitoring and telerehabilitation devices for hand rehabilitation that can provide real-time feedback on hand movements and facilitate home-based therapy. The use of such devices has the potential to improve patient engagement through their interactive interfaces, a

strong predictor of rehabilitation success [4], [12], offering cost savings for healthcare services, increase therapy intensity, and ultimately enhance rehabilitation outcomes [4], [13]–[15].

To assess a patient's hand function, several meaningful concepts are considered, including motor and sensory function, pain sensation, joint Range of Motion (ROM) and balance, grasp patterns, grasp patterns and strength, object handling, and fine hand use [16], [17]. Accurately measuring and quantify the progress made in hand rehabilitation is crucial for effective treatment planning and evaluation. Without proper quantification, it becomes challenging to determine the effectiveness of different rehabilitation methods and interventions, hindering the ability to tailor therapies to the individual needs.

Therefore, the broad objective of this work is to address the persistent challenge of improving upper limb function in stroke patients faster, despite the extensive research conducted on rehabilitation interventions. To address this challenge, a sensorised object was developed, and its embedded sensors were systematically designed, fabricated, and characterised. Subsequently, the system was integrated with LabVIEW, facilitating a user-friendly and quantitative interface. This interface holds the potential for therapists to effectively utilise the system, providing them with the ability to understand the patient's needs more easily, ultimately assisting healthcare professionals in streamlining the customisation of therapy exercises right from the outset of the process.

Furthermore, beyond its significance in stroke rehabilitation, this project recognises the broader implications of measuring hand grasping force. This measurement holds substantial value in multiple domains, including rehabilitation, robotics, prosthetics, and neuroscience [18]. By exploring this aspect, the author aims to contribute to advancements in understanding and treating not only stroke recovery but also wider areas of research and innovation.

1.2 Thesis Structure

This thesis consists of five chapters, organized in sequence to provide a comprehensive understanding of the conducted research. Chapter 2 commences with a literature review covering hand rehabilitation traditional devices, new technologies, sensors, and their efficacy in stroke rehabilitation. It also identifies current gaps and limitations, followed by outlining the main objectives of this study.

Chapter 3 provides a comprehensive account of the design considerations and manufacturing process for the Pneumatic Sensing Chambers (PSCs) developed. This includes detailing the design approach and optimised parameters aimed at ensuring an airtight cavity through 3D printing. The chapter encompasses both theoretical and experimental testing methodologies, followed by a thorough analysis and characterization of the sensors.

In Chapter 4, a deep dive is taken into the development of the object, encompassing its calibration procedure, system architecture, and communication mechanisms. Elaboration

is provided on the complexities of the calibration process and the overall setup of the system.

This thesis ends with Chapter 5, where the research conclusions are summarised, limitations are highlighted, and suggestions for future work are presented.

2

Literature review

Hand rehabilitation methods present a vast and intricate realm filled with immense technological possibilities and challenges that must be overcome. Within the context of hand rehabilitation for stroke patients, numerous methods exist. These include conventional approaches such as occupational therapy, and physical therapy, as well as emerging innovative techniques and commercially available devices that are currently undergoing clinical experimental studies. Examples of these new methods include robotics, virtual reality, telerehabilitation devices, cellular therapy, and others [13], [14], [19]. Despite the variety of approaches available, there is still a significant gap when it comes to quantitatively measuring patients' progress in rehabilitation therapy. The field is far from having a universally accepted system for quantifying and classifying hand functional improvement [20]. This lack of a standardised system hinders the ability to confirm and validate the effectiveness of each emerging therapy method in improving patient outcomes. Despite the efforts made in this field, remains a pressing need to address the challenge of developing a classification system that can help us understand the beneficial impacts of each therapy method. The objective of this chapter is to provide an overview of the current state of knowledge regarding quantitative tools for assessing hand rehabilitation in stroke patients including a brief description of the anatomy and mechanics of the hand, traditional methods, hand rehabilitation devices able to assess features, and sensorised objects. Additionally, it aims to identify existing gaps in this area and propose potential solutions to bridge those gaps.

2.1 Hand Muscle Anatomy and Mechanics

The human hand's anatomy showcases great complexity with a intricate network of distinct muscle groups, each under the guidance of a diverse array of motor and sensory nerve pathways, and all interconnected within the central nervous system [21]. Its intricate structure, coupled with its remarkable dexterity and sensitivity, enables us to perform an exceptional range of tasks, from delicate writing and soldering tasks to powerful feats of strength.

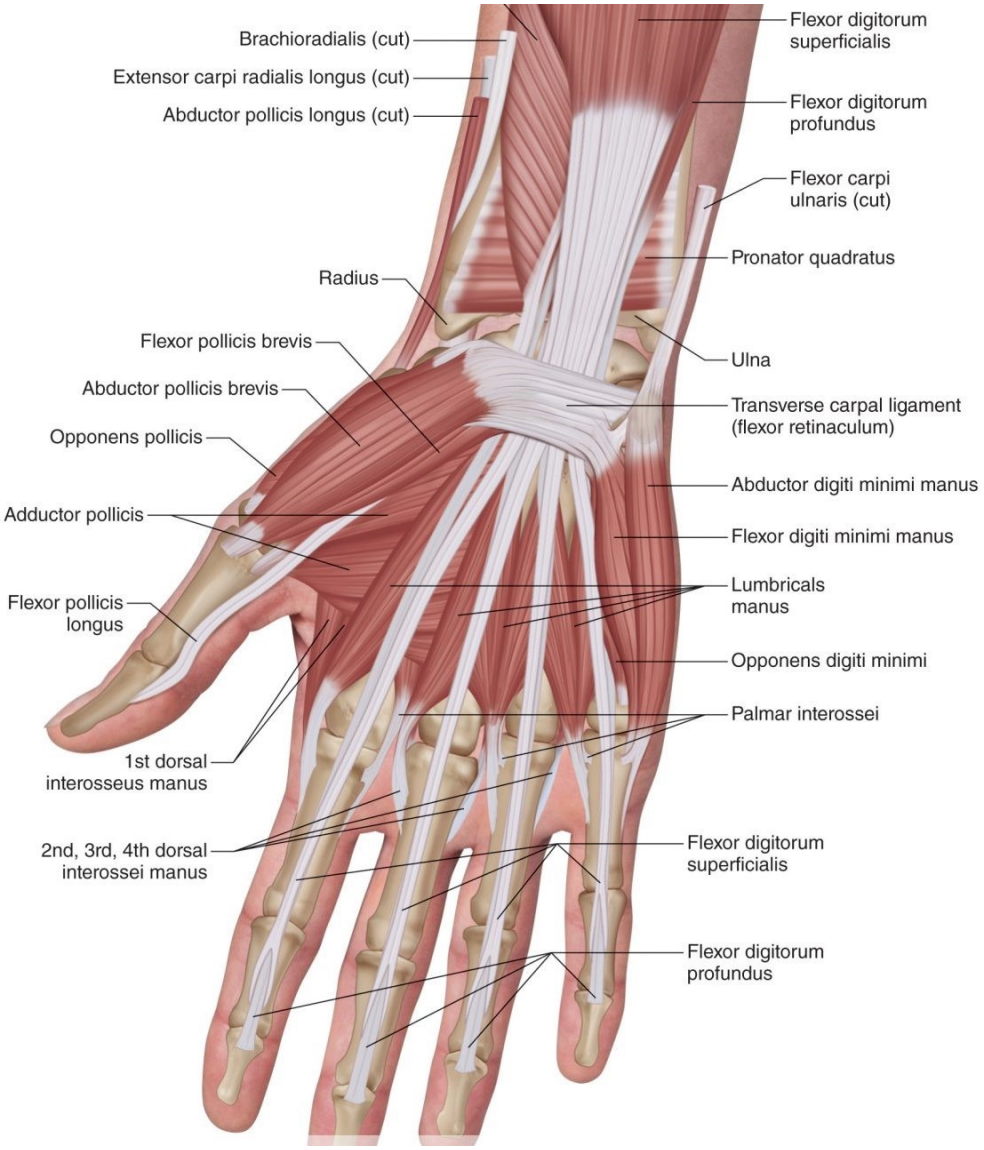

Figure 2.1: Hand Muscle Anatomy [23]

Most of the muscles responsible for hand and wrist movement are situated in the anterior and posterior compartments of the forearm. These muscles, known as extrinsic muscles, play a significant role in enabling a strong grip. In contrast, intrinsic muscles are positioned within the hand itself and are responsible for executing fine motor functions with precision [22]. Together, these muscles collaborate in coordination with a sophisticated bone and joint framework, contributing to the intricate functionality of the hand.

Comprehending hand and finger movements presents a significant challenge, due to their complex reliance on muscles and the intricate interplay among tendons, ligaments, and neural connections. This complexity further complicates the assessment of rehabilitation progress.

Table 2.1 provides a comprehensive overview of the muscles responsible for the hand's

grasping motion, delineating their precise functions, while Figure 2.1 illustrates the schematic and locations of each muscle. By delving into the nuanced roles and placements of each muscle and grasping the distribution of finger forces, this research aims to provide valuable insights to therapists, enabling them to pinpoint gaps in the patient's hand function throughout the rehabilitation journey. Ultimately, the goal is to facilitate the customisation of exercises for each patient, thereby enhancing the effectiveness of treatment interventions, streamlining the process, and improving overall outcomes.

Table 2.1: Hand Muscles: Function, Names, and Specific Actions [22]

Muscle Name	**Specific Actions**
Abductor Pollicis Brevis	Wrist extention, thumb Carpometacarpal (CMC) joint abduction, and extension
Abductor Pollicis Longus	Wrist extention, thumb CMC joint abduction, and extension
Adductor Pollicis	Thumb adduction
Extensor Carpi Radialis Brevis	Wrist extention and abduction
Extensor Carpi Radialis Longus	Wrist extention and abduction
Extensor Carpi Ulnaris	Hand extention and adduction at the wrist joint
Extensor Digitorum	Metacarpophalangeal (MCP), and Interphalangeal (IP) joint of digits and wrist extension
Extensor Indicis	Finger 2 extention
Extensor Pollicis Brevis	Wrist and thumb CMC joint extention
Extensor Pollicis Longus	Wrist and thumb IP, MCP, and CMC joints extention
Flexor Carpi Radialis	Hand flexion and abduction
Flexor Carpi Ulnaris	Wrist flexion and adduction
Flexor Digiti Minimi Brevis	Finger 5 flexion
Flexor Digitorum Profundus	Distal Interphalangeal (DIP) joints of digits flexion
Flexor Digitorum Superficialis	Wrist, MCP and Proximal Interphalangeal (PIP) joints of fingers 2-5 flexion
Flexor Pollicis Brevis	Thumb MCP joint flexion
Flexor Pollicis Longus	Wrist, MCP, and IP joint of the thumb flexion
Lumbricalis	MCP joint flexion, and IP joints extension
Opponens Digiti Minimi	Finger 5 opposition
Opponens Pollicis	Thumb opposition and pronation
Palmaris Brevis	Wrinkles the skin, palmar grip

2.2 Traditional Methods to Access Hand Rehabilitation

The classification of conventional hand therapy typically involves the utilisation of scales and questionnaires that rely on global measurements developed by professional medical associations [10], [20], [24]. However, there is currently no standardised global approach for assessing rehabilitation progress [20].

Stroke severity in patients is commonly assessed by professionals using scales such as the Chedoke-McMaster Stroke Assessment (CMSA) or the National Institutes of Health Stroke Scale (NIHSS) [24]. Motor functioning assessments are then categorised using scales like the Fugl-Meyer Assessment (FMA). The FMA scale is a 226-point measure of stroke recovery Hemiplegia, grouped into 5 domains: motor function, sensory function, balance, joint ROM, and joint pain. Each domain has items scored on a 3-point scale (0 = cannot perform, 1 = partially, 2 = fully). Motor domain covers upper and lower extremities (max 100 points). Other domains have their maximum points as well: sensation (24), balance (14), ROM (44), and joint pain (44). A trained physical therapist conducts a one-on-one analysis of the questionnaire, typically requiring approximately 30 minutes for each patient [16]. FMA scores are highly prevalent and serve as a key measure to assess the effectiveness of rehabilitation devices [7], [16], [19], [20].

In hospitals, other commonly used methods for obtaining quantitative measurements of hand rehabilitation include goniometers [25] and hand-held dynamometers [26]. Goniometers are employed to measure the angles between two body parts and can assess hand joint angles. Dynamometers are useful for measuring the strength and function of muscles and joints, providing valuable information about the overall hand strength of the patient.

Other scales and manual tests, such as Brunnstrom's motor recovery stage, the Manual Function Test, and the Box and Block Test, are also used to evaluate patient function.

2.3 Hand Rehabilitation Devices

Typically employed in rehabilitation training, these devices are classified into active, passive, and assistive rehabilitation types. However, this literature review focuses on devices that possess the most comprehensive set of features, specifically highlighting the wide range of measurements each device can assess.

A recent article [10] comprehensively reviewed the current technological solutions available for hand rehabilitation, including emerging options that have been implemented in hospitals in recent years to track hand function progress. These solutions encompass a wide range of commercially available robotic devices, such as exoskeletons and end-effector devices, which utilise interactive games, augmented reality, or virtual reality to facilitate hand rehabilitation [10]. While exoskeletons are versatile devices that assist with repetitive movements and provide overall rehabilitation training for larger body parts, end-effectors specifically target finger rehabilitation and are controlled by the DIP joint

[20]. It is worth noting that end-effector devices are, in most cases, immobile because they require the hand to be held in place in order to accurately control the movement of the distal DIP joint. This means that the hand cannot move freely while using these devices. While portable options like exoskeletons do offer the advantage of remote rehabilitation for patients, they may have limitations in terms of the range of rehabilitation exercises they can support and the ability to track progress effectively [20]. End-effector devices provide a higher degree of control and feedback compared with exoskeletons. Moreover, since these devices don't prioritise portability, they have more freedom to incorporate a greater number of sensors. It is important to consider both the benefits of portability and the potential trade-offs in terms of rehabilitation possibilities and progress monitoring when selecting a device.

For instance, the Tyromotion's Amadeo device [27], is an end-effector device designed for hand and finger rehabilitation. It provides precise and controlled exercises with its five degrees of freedom, allowing independent finger movement and passive rotation joints. The device is equipped to assess crucial metrics such as ROM, Force, and Spasticity, and it is particularly effective for patients with mild stroke.

Gloreha [28] is an exoskeleton device that utilises pneumatic actuators and a cable-driven system to enable finger movement. It captures essential data such as active and passive ROM, movement speed, coordination, and advancements in task execution.

CyberGrasp [29], by CyberGlove Systems, is a lightweight exoskeleton glove for virtual reality rehabilitation. It utilises a linkage system and Force Sensing Resistor (FSR) for safe rehabilitation, allowing users to interact with virtual 3D objects. It is also portable for different workplace environments.

(a) Amadeo [27] (b) Gloreha [28] (c) CyberGrasp [29]

Figure 2.2: Hand Rehabilitation Devices

2.4 Sensorised Objects

Sensorised objects emerged as the necessity to overcome the drawbacks of the exoskeletons and gloves. Some sensorised objects have been found in the literature to access grasping force measurement in the context of hand rehabilitation and robotic hand performance, however, no commercial available sensorised object was found.

In their study, Kõiva et al. [30] introduced iObject, a tactile sensor-based system comprising 220 resistive sensors to detect contact pressure location and force during human

and robotic hand grasping. In addition, iObject possessed the ability to wirelessly detect both object acceleration and orientation over a Bluetooth connection. This technology was subsequently utilised by Roa et al. [31] to quantify human grasp through objective measurements. This work provided valuable insights into the quantitative assessment of human grasping capabilities with the aim to increase robotic grasp robustness.

Romeo et al. [32] developed a FSR spherical object designed to quantify human performance in the tripod grasp. This innovative object featured three contact areas and integrated an accelerometer to detect slip, with all the hardware cleverly contained within the sphere. Only the cables for power supply would extend externally, resulting in an exceptionally compact and streamlined device.

In another investigation, Cordella et al. [18] developed a cylindrical object equipped with sixteen piezoresistive sensors to evaluate grasping performance in both human and robotic hands. The object was divided into 16 flexible tabs, allowing for independent measurement of each finger's force. Additionally, it incorporated a Inertial measurement unit (IMU) to accurately track the object's orientation. The device also featured wireless communication capabilities, facilitating seamless data transfer.

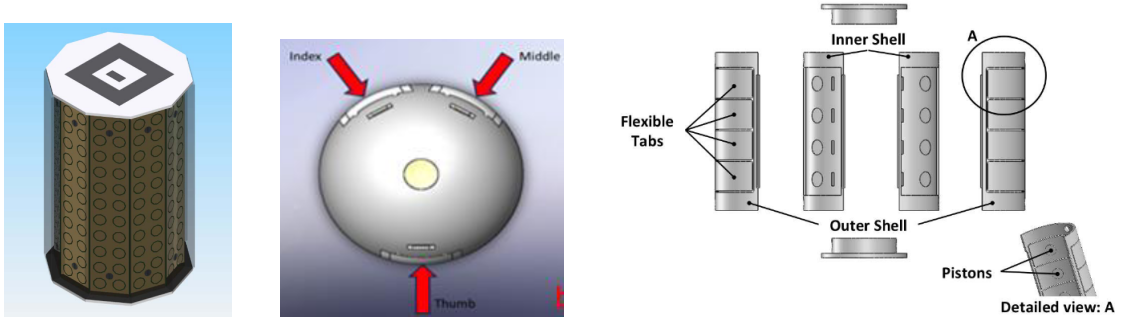

(a) iObject [30] (b) Tripod Grasp [32] (c) Cylindrical object with 16 piezoresistive sensors [18]

Figure 2.3: Sensorised Objects

2.5 Overview of Sensor Technologies

Recently, there has been increasing interest in the development of tactile sensors, with various options being proposed, including capacitive, resistive, and more recently, pneumatic sensors. The Table 2.2 presents a comprehensive comparison of the main advantages and disadvantages of the three prominent systems that have been extensively studied for their application in the field of tactile sensors.

It is crucial to emphasize that the specific implementation, design, and intended use of a sensor can have a substantial impact on the parameters mentioned in Table 2.2. Different manufacturing procedures may have variations, resulting in variations in performance characteristics among tactile sensors. Therefore, it is imperative to carefully consider these factors when choosing a tactile sensor for a specific application.

Table 2.2: Comparison of Various Sensors [18], [30], [32]–[37]

Parameters	**Resistive**	**Capacitive**	**Pneumatic**
Flexible	High	High	High
Hysteresis	Low	High	High
Sensitivity	High	Low	High
Linearity	Moderate	High	High
Accuracy	Moderate	Moderate	High
Cost	Moderate	High	High
Sensitive to Interference	Moderate	Moderate	High
Circuit Complexity	High	Low	High
Response Time	Moderate	High	High

2.6 Limitations in Current Devices and Methods

Based on a comprehensive review and careful analysis of the insights provided by the aforementioned studies, several limitations and existing gaps can be identified.

The commonly used FMA scales, while widely utilised, suffer from subjectivity and lack of meaningful quantitative data on progress [38]. Additionally, they can yield substantial variability without the previous experience and expertise from a healthcare professional [20]. Moreover, they can be time-consuming, necessitating the presence of a professional for a period of 30 minutes [16]. Goniometers, although used for measuring joint angles, encounter accuracy issues due to challenges in positioning and reading measurements, along with the time-consuming nature of assessing multiple joints. Dynamometers, while useful for measuring overall hand strength, lack the ability to assess individual finger performance, which is crucial for targeted and personalised hand rehabilitation.

Commercial hand rehabilitation devices, although available, often focus on finger force instead of grasping force, which may not fully capture the intricacies of hand functionality. Furthermore, these devices tend to be expensive, bulky, and require dedicated space for their operation. Additionally, a therapist is typically needed to oversee and control the system, which can be time-consuming and inefficient, especially for patients with severe impairments [10]. For stroke patients, wearability is also a concern due to varying levels of impairment. Despite efforts to design adaptable gloves and accommodate different hand sizes, achieving precise calibration with hand joints remains a significant challenge. Inaccurate calibration can lead to measurement errors and hinder the effectiveness of rehabilitation efforts for certain patients [18].

In the case of the Amadeo [27] device, while it offers advanced features and precise finger rehabilitation, it shows limitations in severe stroke cases. Its availability primarily in medical institutions and the high cost, up to $ 100,000, can also restrict its accessibility. Similarly, the CyberGrasp [29] device, with its complex structure, is associated with a

significant cost of $ 6000, which can restrict its affordability for certain users.

In response to the limitations associated with exoskeletons and end-effector devices, sensorised objects have emerged as promising alternatives, providing practicality, versatility and a lower production cost. These objects are equipped with robust sensors that prioritise accuracy and durability, addressing the shortcomings of traditional approaches for grasping force measurements. However, it is worth noting that commercially available sensorised objects are currently limited, and there are still some drawbacks that need to be addressed in order to fully harness their potential.

The device introduced by Koiva et al. [30] has high sensor resolution but can not measure finger force contribution independently. Similarly, the design presented by Romeo et al. [32] has fixed contact areas, limiting grasping options to match the sensorised areas. Cordella et al. [18] explored independent finger measurements, but fixed contact remain a limitation. Another device discussed in the literature review by Gao et al. [39] lacked the ability to measure grasping force intensity. These limitations emphasise the need for more advanced and comprehensive rehabilitation methods that address individual finger measurement, flexibility, accurate force measurement, and personalised approach to stroke rehabilitation.

2.7 Project Aims

Through comprehensive review and meticulous analysis of the aforementioned studies, this project aims to develop a sensor-equipped telehealth device, specifically tailored for stroke patients. The device aims to present an innovative and quantitative approach to evaluating outcomes, while simultaneously addressing the limitations previously identified. The objective is to create a cost-effective, accurate, and versatile sensorised object that assesses hand grasping force intensity and distribution. By utilising this object, the therapist should be able to track stroke patients' progress in hand force during rehabilitation and enable personalised rehabilitation pathways by identifying any deficiency in finger force within specific muscles or joints.

The proposed device is based on a cylindrical object, incorporating PSCs to capture hand and finger grasping force, dexterity, and provide real-time feedback to the user. PSCs were chosen for this application due to their demonstrated simplicity, cost-effectiveness, and technical advantages, such as high sensitivity, low hysteresis, and rapid response time [35], [40]. The device was designed to be portable, easy to use in both healthcare and home environments, versatile to various hand sizes, and adaptable to individual abilities and impairment severity levels.

This project is divided to address three different aspects towards improvement and standardisation of hand rehabilitation solutions:

1. Strategise, conceptualise, construct, and evaluate a novel PSC aligned with the objectives of the sensorised object.

2. Plan, design, fabricate and assemble a sensorised object integrated with pressure sensors to accurately measure and analyse the intensity and distribution of grasping force.

3. Develop an interactive system that facilitates seamless communication between the object, an interface, and the user. This system should be capable of capturing data during hand-object interactions, displaying hand and finger grip force in real time on a screen, enabling therapists to observe these movements, and facilitating data downloading for in-depth analysis when necessary.

Figure 2.4 depicts a schematic of the main stages of prototype development, encompassing the PSCs and cylinder design, the assembly process, and the LabVIEW interface.

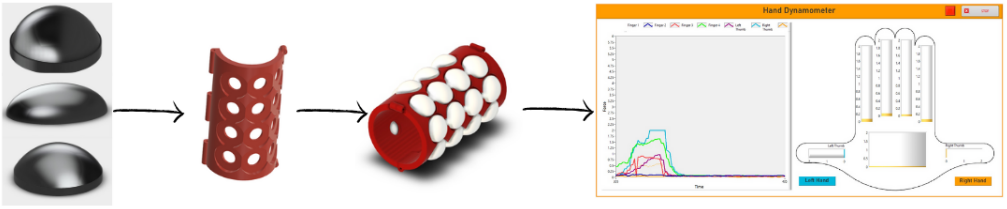

Figure 2.4: Schematic of the prototype developed and the LabVIEW software

3

Sensor Development and Characterisation

3.1 Design Considerations and Sensor Manufacturing

3.1.1 Design Principles

The PSCs were modeled in Autodesk Fusion 360, with approximately 10 different shapes ranging from rectangular to half-spherical. However, only 3 designs were ultimately tested due to specific design requirements that needed to be met. Figure 3.1 illustrates three designs: S2, the first larger sphere; E1, the small half ellipsoid, and S1, a small half sphere with the same inner volume as E1. The labels "1" and "2" serve the purpose of distinguishing between the designs based on their volume. Here, "1" corresponds to the smaller volume, while "2" corresponds to double the volume of the former.

To meet the design requirements, the object needed to be graspable by the patient

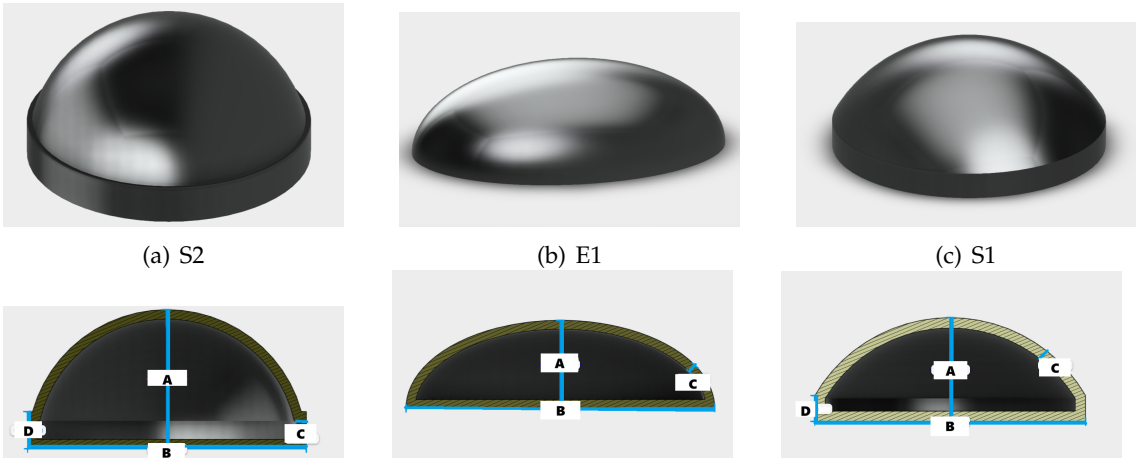

(a) S2 (b) E1 (c) S1

(d) S2 Sizes - A: 15mm, B: 30mm, C: 1mm , D: 4mm

(e) E1 Sizes - A: 10mm, B: 35mm, C: 1mm

(f) S1 Sizes - A: 10mm, B: 26mm, C: 1mm, D: 2.5mm

Figure 3.1: Schematic of the PSCs design improvements from the oldest version (a) to the most recent one (c) and correspondent sizes

and capable of accurately measuring pressure regardless of the grasping method. Consequently, designs with sharp edges and high-stress areas were avoided due to their misalignment with the original design principles. To prevent air leakage, a minimum wall thickness of 1mm was used. The dimensions of all sensors were capped at 30 x 30 x 15 mm to achieve a harmonious equilibrium between sensitivity and resolution.

3.1.2 3D Printing

The 3D Computer-Aided Design (CAD) designs were sliced in a commercial 3D printing software, Simplify3D (Simplify3D LLC, OH), using an imported parameter process optimised in [41] to use flexible filaments. To improve printing quality and prevent air leakage in spherical shapes, additional adjustments were made, specifically tailored to these particular shapes. These modifications are outlined in detail in Table 3.1. The resulting files were exported using FlashPrint5 software for use with a FlashForge Inventor (FlashForge Inventor, USA) Fused filament fabrication (FFF) 3D printer with a commercially available Thermoplastic polyurethane (TPU), "Ninja Flex" (Nin-jaTek, USA) with a filament shore hardness of approximately 85A, and an infill percentage of 100 %. Figure 3.2 presents the 3D-printed enhancements achieved through the optimised parameter process.

Table 3.1: Optimized Parameters For 3D-printed Airtight Spherical Surfaces

Parameters	**Value**	**Unit**
Resolution Settings		
Width	0.45	mm
Top Solid Layers	10	
Bottom Solid Layers	4	
Infill Settings		
Internal Fill Pattern	Full Honeycomb	
External Fill Pattern	Concentric	
Internal Fill Angle Offsets	+/-120	º
Outline Overlap	80	%

(a) (b)

Figure 3.2: Improvements achieved through the optimisation of the manufacturing process. (a) Before (b) After

3.2 Methodology

3.2.1 Finite Element Modeling

3.2.1.1 Static Structural Analysis

After the more suitable CAD models were designed, FEA was performed using ANSYS Workbench to obtain a better understanding of the design's performance using hyper-elastic material models. By utilising "Static Structural Analysis", it was possible to compare various 3D CAD models of the soft sensors prior to conducting physical tests. This provided insight into how the shape would perform in terms of sensitivity, i.e. less load for the same displacement output, ultimately saving time and resources. The geometry was directly imported as a .STEP file to "Design Modeler".

3.2.1.2 Material

To perform this analysis, a commercially available TPU known as "Ninja Flex" was imported from the "Engineering Data" library. This material had already been manually defined. The TPU was characterised as a hyperelastic material through the use of The Mooney-Rivlin five-parameter model, which was determined based on the mean stress-strain data obtained from previous experiments [34].

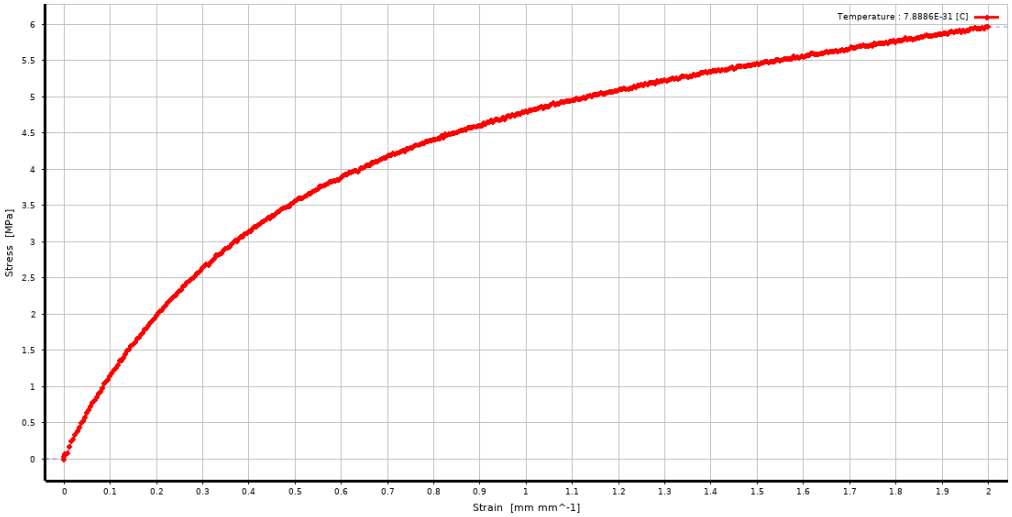

Figure 3.3: Stress-Strain graph obtained from previous experimental tests [34]

3.2.1.3 Meshing

The adaptive mesh technique was used to mesh the geometries, and the "Tetrahedron" method was employed to improve accuracy, increase flexibility, reduce meshing time, and ensure good convergence. This method was particularly well-suited for modeling the curved surfaces required for this application. To achieve a good balance between accuracy and computational processing for this material, the "Body Sizing" parameter was applied

to the Spherical and Elliptical surfaces of the sensors with an element size of 1.2mm. For hyper-elastic materials, a relatively coarse mesh was deemed appropriate due to their ability to undergo large deformations. The adequacy of the mesh size was confirmed by conducting a mesh convergence study, which involved analysing the system with different mesh sizes and ensuring consistency and minimal variation in the results.

3.2.1.4 Boundary Conditions

- **Contacts -** Contact pairs were established automatically for .STEP files that featured a flat surface cylinder and the PSC. These pairs were defined as frictionless, modeling standard unilateral contact for a nonlinear solution where the area of contact changes while the stroke is applied. To prevent convergence issues, the time step controls were configured to use "Automatic Bisection." Additionally, the interface treatment was set to "Adjust to Touch," which enabled a required contact offset to bring the contact region to a state of "just touching."

- **Fixed Support -** A "Fixed Support" is applied to the bottom face of the PSC, which is in contact with the UTM base.

- **Air Pressure -** In this simulation, pneumatic pressure in the air cavity was not considered due to the complexity in Static Structural Analysis of ANSYS which may lead to results different from reality.

- **Remote Displacement -** For .STEP files with only the PSC, a remote displacement was applied normal to the surface and with a 45º angular inclination, with displacements of 2 mm. The different directions were intended to compare the performance of various edges and shapes, studying the relationship between applied displacement and correspondent reaction force.

- **Displacement -** For .STEP files with a PSC and a flat cylindrical surface, a directional displacement was applied to the cylinder, as shown in Figure 3.4, simulating the UTM to record a more realistic result. The spherical surface was set with a free displacement in the same perpendicular direction and constrained with the other two surfaces.

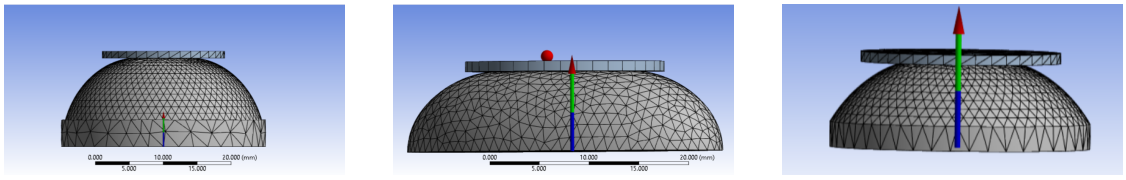

Figure 3.4: FEM Force Reaction With a Flat Surface Stroke of 2mm

3.2.1.5 Analysis Setup

To ensure accurate solutions and control convergence in nonlinear static analyses, the "Automatic Time Stepping" feature is utilised. 10 substeps were selected to divide the analysis into smaller time increments for gradual displacement application, which helps prevent convergence issues. Due to the anticipated large deformations, the "large deflection" option must be enabled to account for geometric non-linearity in the analysis. As structures undergo significant deformation, their stiffness and stress distribution can change considerably, which can significantly impact the analysis results. To stabilise the model and achieve a reasonable solution, the program added "Weak Springs" when frictionless contact was set in the assembly.

3.2.2 Measurement Techniques and Experimental Setup

To assess the accuracy and validity of the sensors in accordance with the FEA results, displacement tests were carried out. The Honeywell ABPDANT005PGAA5 piezoresistive silicon pressure sensor was utilised in all tests due to its exceptional precision, long-term stability, sensitivity, and compact design. As shown in Figure 3.5, the sensor was incorporated into the PSC using a commercially available speedfit water pipe with a fabric airtight glue, and linked to an Arduino NANO microcontroller to read analog data and convert it into pressure readings in kPa.

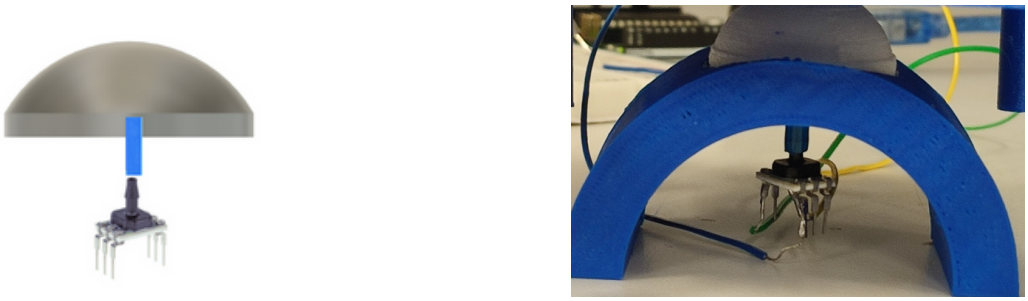

(a) (b)

Figure 3.5: Schematic of the sensor assembling: PSC with speedfit water pipe and pressure sensor

Two types of displacement tests were conducted: static and dynamic. The static test involved the setup depicted in Figure 3.6 (a) to evaluate stability over time, and the dynamic tests were conducted using the EZ-LX Shimadzu UTM as shown in Figure 3.6 (b) to evaluate linearity, hysteresis, repeatability, lifetime, and durability. The software "TrapeziumX" was used to record the deformation and force applied for subsequent analysis. In addition, the output pressure was measured using Arduino NANO and recorded through CoolTerm software.

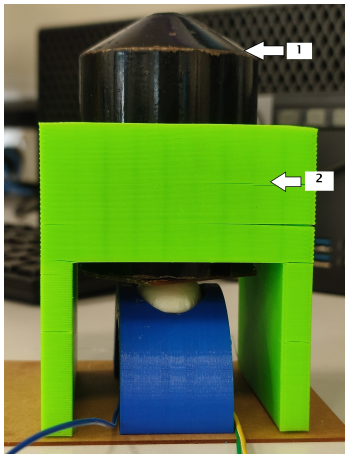

(a) Static weight test - (1) Dead Weight, (2) Additional support

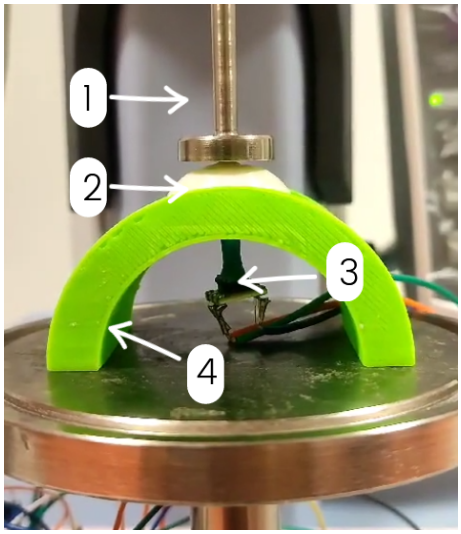

(b) UTM dynamic tests - (1) UTM Cell, (2) PSC, (3) Pressure Sensor, (4) Support

Figure 3.6: Experimental tests setup

3.2.2.1 Stability Over Time

To ensure a consistent flat surface a fixed weight was applied on top of the PSC during the test, an additional support was included as shown in Figure 3.6 (a). The tests were conducted for 30 minutes with a 1 Kg dead weight applied while pressure was recorded. UTM was not employed for this particular test due to its inability to maintain a constant dead load as stable as gravity.

3.2.2.2 Linearity

To study the linearity of the pressure with a constant load, a single load test was performed. Cell load was increased from 0 to 15 N with an increment of 2.5 N and holding 5 seconds to guarantee that the final state pressure was recorded.

3.2.2.3 Repeatability and Hysteresis

In this test, 10 activation cycles were conducted at 2 mm displacement. Throughout all cycles, the displacement cell maintained a speed of 0.1 mm/s and spent 0.5 seconds at both the minimum and maximum displacement positions. The hysteresis curve was obtained by gradually increasing the displacement until it reaches the 2 mm, and then gradually returning to the starting position.

3.2.2.4 Durability

In this test, 500 activation cycles were conducted for a 2 mm displacement. During each cycle, the displacement cell maintained a speed of 4 mm/s and remained at both the minimum and maximum displacement positions for 0.5 seconds.

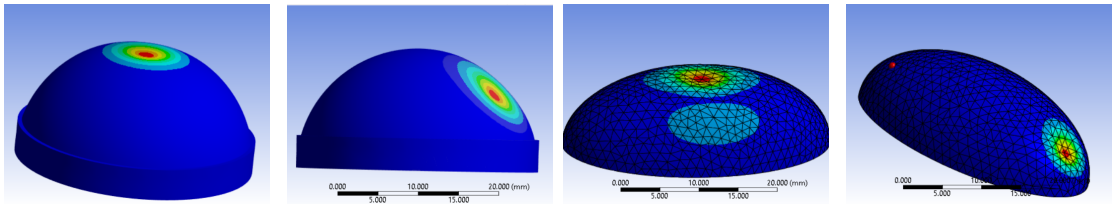

Figure 3.7: FEM With Remote Point Deformation (Directional and Angular) for S2 and E1

3.3 Sensor Characterisation

3.3.1 Finite Element Analysis

As explained in subsection 3.2.1, FEM was conducted using different applied displacements. In this study, force reaction, stress, total deformation and volume changes were analysed.

3.3.1.1 Remote Displacement Analysis

Table 3.2 reports the reaction force and maximum stress point observed when a 2 mm remote displacement with different angles was applied, as presented in Figure 3.7.

This test was designed to assess the performance of different shapes in terms of reaction force and stress when they underwent compression from directions other than the perpendicular one, analysed from an analytical perspective. The objective was to identify a shape that could ensure consistent force application to the sensor surface, regardless of how it is grasped. Consequently, the ideal shape would exhibit minimal discrepancies between directional and angular forces.

Table 3.2 indicates that applying a normal displacement of 2 mm across all shapes yields comparable reaction forces and maximum stresses of approximately 1.6 N and 1.1 MPa, respectively. However, for angular displacements, distinct outcomes are observed. Specifically, the elliptical shape's edge yields a higher reaction force of 3.4 N compared to the reaction forces of 1.9 N for spherical shape S2 and 2.2 N for spherical shape S1.

Table 3.2: FEM Comparison Between Shapes With Perpendicular and 45º Angles Applied With Pinball

	Force (N)			**Stress (MPa)**		
	S2	**E1**	**S1**	**S2**	**E1**	**S1**
Directional	1.6	1.6	1.6	1.2	1.1	1.1
Angular	1.9	3.4	2.2	1.3	2.1	1.3

This outcome arises from the higher stress experienced on the elliptical surface when compressed at the lateral edge. By manually measuring the diameter corresponding to the circular area deflected at each angular deflection using the "Probe" tool in ANSYS Workbench, a relationship can be discerned. This result could have been anticipated due

to the higher stress point of shape E1, corresponding to 2.1 MPa, when compared with the maximum stress points of 1.3 MPa for S1 and S2. This dependence is a consequence of the shape itself. Upon deflection, E1 presents a circular deflection of 8.96 mm, while S1 exhibits a deflected circular surface with a 10.3 mm diameter, and S2 with 11.8 mm.

The total deflected area is larger for S2, followed by S1, and lastly, E1, which has the smallest deflected area. Considering the equation:

$$\sigma = \frac{\text{Force}}{\text{Area}} \tag{3.1}$$

Stress is dependent on force and surface area. As E1 has a smaller deflected area, the distribution of forces is concentrated, leading to an increase in the overall reaction force.

The difference between the directional and angular reaction forces is more pronounced in the case of the E1 shape, indicating it to be less promising. This discrepancy could result in inaccurate predictions of the grasping force, depending on how the patient grips the object. In this test, S2 and S1 emerged as the more suitable options.

3.3.1.2 Flat Surface Displacement Analysis

Figure 3.8 depicts the resulting solution from the application of a 2 mm displacement to the models' spherical and elliptical surfaces, thus simulating the UTM.

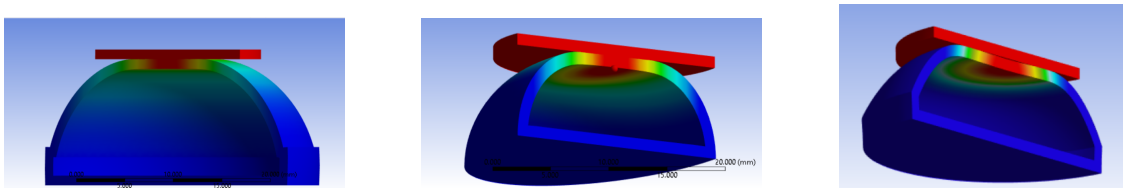

(a) S2 (b) E1 (c) S1

Figure 3.8: FEM With Flat Surface Deformation Simulating UTM

To compare the relationship between the experimental values with the FEM and to understand its accuracy, the graph from Figure 3.9 presents the linearity between V_1/V_2 and its corresponding pressure over displacement. P_1 and V_1 are the initial pressure and volume, respectively, and P_2 and V_2 are the pressure and volume after corresponding displacement, respectively. The internal volume was measured directly from the CAD designs every 0.25 mm of displacement of the FEM simulations, as shown in Figure 3.9. This relationship can be described as the inverse relationship between pressure and volume of a gas at constant temperature, which is known as Boyle's Law [42] given by the equation:

$$P_1V_1 = P_2V_2 \tag{3.2}$$

Figure 3.9 illustrates the relationship between the output pressure and the corresponding displacement, as well as the linear correlation between the FEM results of volume change of the different shapes. In the linear fit of S2 results both, relationships resulted in a coefficient of determination of $R^2 = 0.969$ for the FEM data and $R^2 = 0.982$ for the

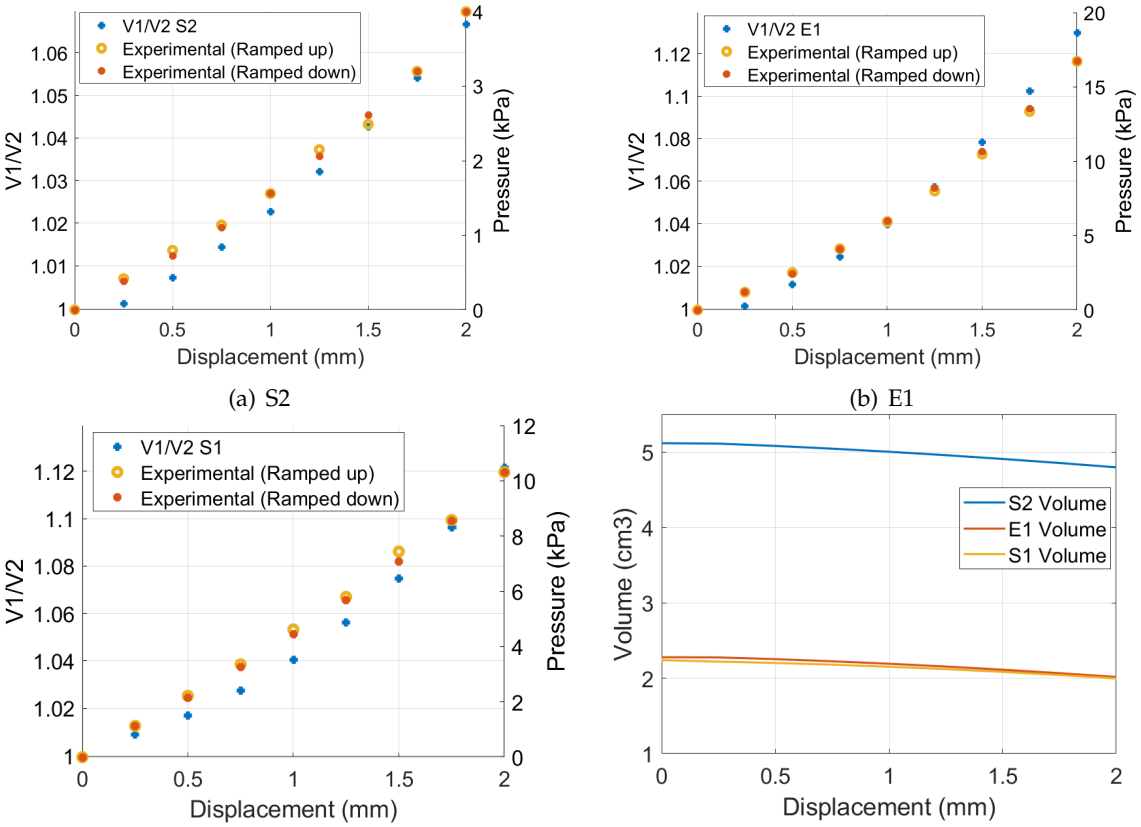

(a) S2 (b) E1

(c) S1 (d) Comparison of volumes between shapes

Figure 3.9: Linearity between FEM volume ratio and experimentally measured relative pressure

experimental data. Similarly, E1 presented a coefficient of determination of $R^2 = 0.954$ for the FEM data and $R^2 = 0.972$ for the experimental data. For S1, $R^2 = 0.963$ was obtained for the FEM results and R^2 =0.996 for the experimental results. The primary objective of this graph is to provide evidence of the accuracy of the developed FEA. Due to the small size of the PSC and the minute displacements under study, even the slightest variation can result in higher variances, which can explain the more pronounced disparities observed between FEM and experimental results when subjected to smaller displacements. Although there may be multiple reasons for the small difference observed between FEM and experimental results, the most significant factors could be attributed either to the starting point used in the UTM or to the material properties used in FEM. Nonetheless, it is noteworthy that despite these variations, there is a notable alignment between the experimental and theoretical outcomes.

3.3.2 Experimental Results and Discussion

This study aims to analyse and compare the force and stroke applied with the corresponding output pressure to identify the optimal solution. The desired outcome is a higher pressure variance for the displacement achieved with minimum force required.

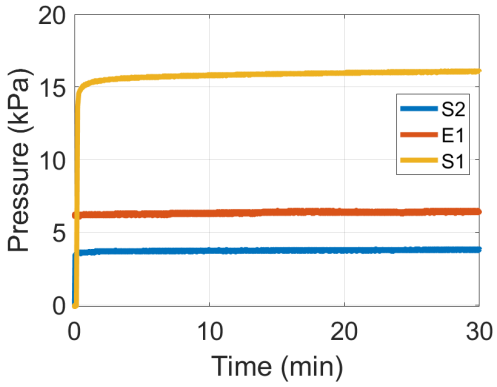

Figure 3.10: Relative pressure of stability over time experimental tests

3.3.2.1 Stability Over Time

Figure 3.10 illustrates the results of the stability over time test, which demonstrate consistent readings over the 30-minute test duration with 1 Kg dead weight was applied. There was an increase in readings during the first minute, which could be attributed to the relaxation effect of the material. Nonetheless, after 2 minutes, no more considerably oscillations were recorded, indicating good stability of the PSCs. The stable signals validate the air-tightness of the system, ensuring that the collected data is both reliable and consistent, which is crucial for the effectiveness of PSCs.

3.3.2.2 Linearity

Figure 3.11 depicts the relationship between the sensors' pressure readings and the applied load. To ensure the accuracy of the results, a waiting time of 5 seconds was observed before recording the final state pressure value that corresponded to the applied load. The linear fit was applied in MATLAB tools to show the best fit. All shapes exhibited good predictability with a coefficient of determination of R^2 = 0.9928 for S2, a coefficient of determination of R^2 = 0.9618 for E1 and finally a R^2 = 0.9908 for the S1. It can be observed a more predictable behavior for the S2 and S1 spheres, as evidenced by their very high coefficient of determination, making them more favorable in this test. As anticipated, the large spherical shape exhibits lower sensitivity compared to the other two shapes, owing to its larger inner volume. Nevertheless, upon subjecting the shapes with an equivalent inner volume to the same load, a noticeable pressure variation is apparent in the S1 shape (0 to 25 kPa) compared to the E1 shape (0 to 13 kPa).

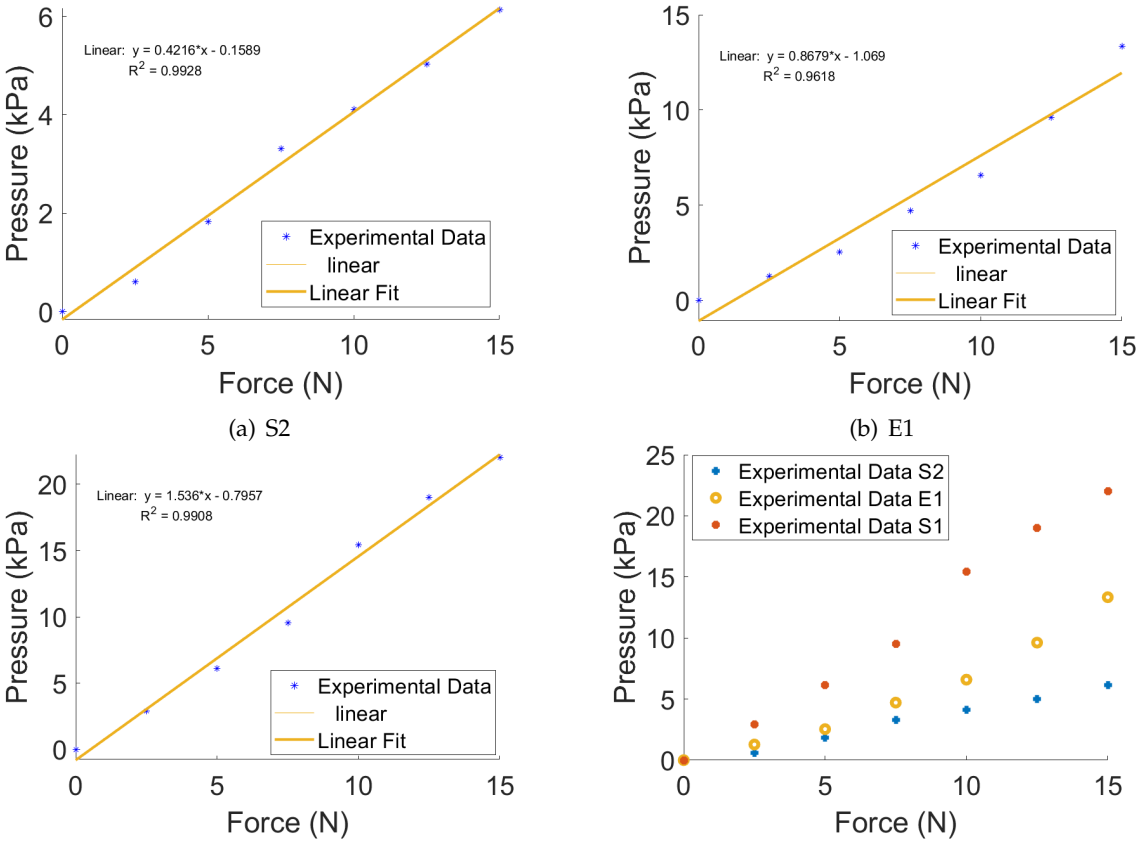

(a) S2 (b) E1

(c) S1 (d) Comparison between shapes

Figure 3.11: Linear Regression of relative pressure in Static Weight Test results

3.3.2.3 Repeatability

As explained in Section 3.2.2, this test was run over 10 cycles, with the UTM lifting up and down with a speed of 0.1 mm/sec and holding in each maximum positions for 0.5 seconds. The pressure change in E1 is notably higher compared to S1 for the same displacement, as observed in Figure 3.9. This variation is possibly attributed to the higher V_1/V_2 ratio of E1 (1.13) when compared with S1 (1.12). Although the initial internal volume of both the E1 and S1 is the same, a greater variation is observed in the inner volume of the ellipsoid when compressed with the same displacement. Figure 3.12 provides compelling evidence that the PSCs present high degree of repeatability, exhibiting reliable pressure signals without any discernible drift. These outcomes reinforce the air-tightness of the PSCs, which is crucial for soft robotic applications requiring precise monitoring and control of repetitive movements.

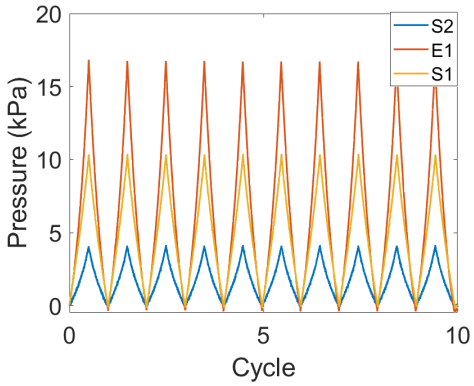

Figure 3.12: Relative pressure of repeatability experimental tests

3.3.2.4 Hysteresis

Figure 3.13 depicts the output pressure measured from the PSCs as the displacement was ramped up and down. Notably, the hysteresis curve of all PSCs displayed negligible hysteresis, which is crucial in avoiding errors and instability in the control system. As presented in subsection 3.3.2.2, spheres exhibit a simpler and more predictable behavior when compared with ellipsoid coefficient of determination, noticeable in Figure 3.13.

Accurate and reliable sensing play a crucial role in soft robotics as these devices are designed to interact with humans. In this regard, minimal hysteresis is crucial to ensure consistent and responsive feedback signals, especially during rapid or unpredictable movements of the patient. The results obtained align with the existing literature [35], [41], demonstrating the effectiveness of such sensing mechanisms. These findings highlight the importance of reliable sensing in soft robotics and its potential to improve patient care and comfort.

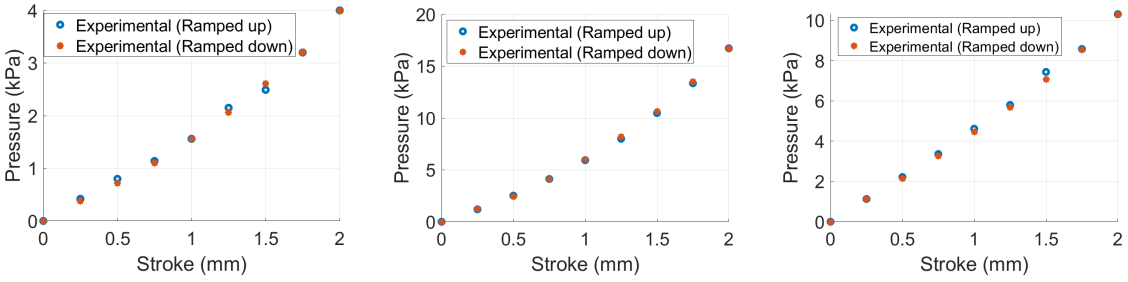

(a) S2 (b) E1 (c) S1

Figure 3.13: Hysteresis Curve reading relative pressure

The displacement and correspondent force in both FEM and experimental results is presented in Figure 3.14. When considering the force required to generate a specific output pressure, it is observed that spherical shapes require less force compared to ellipsoids for the same displacement. However, in the case of S1 and E1 having the same inner volume, a significantly greater force is required for E1 to achieve the same pressure variation. As a consequence, it is evident that the small sphere is the superior shape in this scenario.

The influence of stiffness in S2 is apparent in the data. The experimental results show a smooth curve for S2, which can be attributed to the walls of S2 offering increased resistance beyond 1.5mm of compression. This leads to two distinct reaction force behaviours: the first one with a smaller linear slope up to 1.5mm, and the second one with a steeper linear slope beyond that threshold.

In contrast, both E1 and S1 exhibit a simpler and more predictable behaviors. While the coefficient of determination for the experimental results corresponds to 0.942 and 0.925 for the ramped-up and ramped-down results of shape S2, E1 presented $R^2 = 0.997$ and $R^2 = 0.981$ for the ramped-up and ramped-down phases, respectively. For shape S1, $R^2 = 0.980$ for the ramped-up phase and $R^2 = 0.995$ for the ramped-down phase.

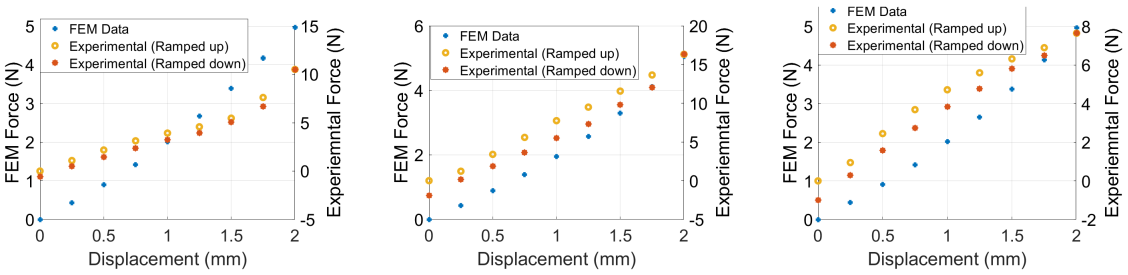

(a) S2 (b) E1 (c) S1

Figure 3.14: Comparison of force over displacement between FEA and experimental results

With reference to FEA results in Figure 3.14, E1 has a higher reaction force, when compared with the other shapes. That difference is very reduced when compared between experimental results. In the blue markings, it is possible to compare the FEA results. Although there is still a noticeable difference in reaction force for E1 compared to the other shapes, this difference is significantly reduced when compared to experimental results. This is because the pneumatic pressure inside the cavity is not taken into account in this static structural analysis, resulting in analytical results that are much smaller than reality. Furthermore, this problem was exacerbated by the low-quality exhibited in the manufacturing process, compounded by challenges in the FFF printing process using flexible filaments and difficulties in printing spherical surfaces. Upon sectioning one PSC and measuring its thickness with a caliper, higher thickness was found in certain regions of the component, particularly on the top spherical surface, as presented in Figure 3.15.

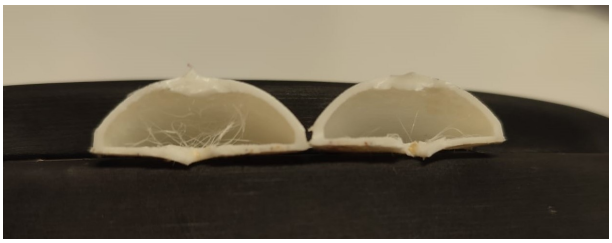

Figure 3.15: PSCs sectioned

Additionally, discrepancies between FEA and experimental results can be attributed

to differences in the material parameters used to define Ninja Flex in ANSYS compared to the Ninja Flex filament.

It is also difficult to draw direct comparisons with existing research, given the sensitivity's dependence on various factors such as inner volume, thickness, and transducer sensitivity, which vary depending on the application. Nevertheless, the small sphere shape appears to be a promising and effective solution in this context. Its compact size and superior sensitivity make it a compelling choice for a broad range of applications in biomedical engineering field.

3.3.2.5 Durability

The displayed data in Figure 3.16 illustrates 500 activation cycles with no observable drift. All shapes presented great consistence over the 500 cycles serving as compelling evidence that the PSCs exhibit remarkable robustness, thereby enhancing the overall reliability and performance of the system, while also reducing maintenance costs and minimizing downtime.

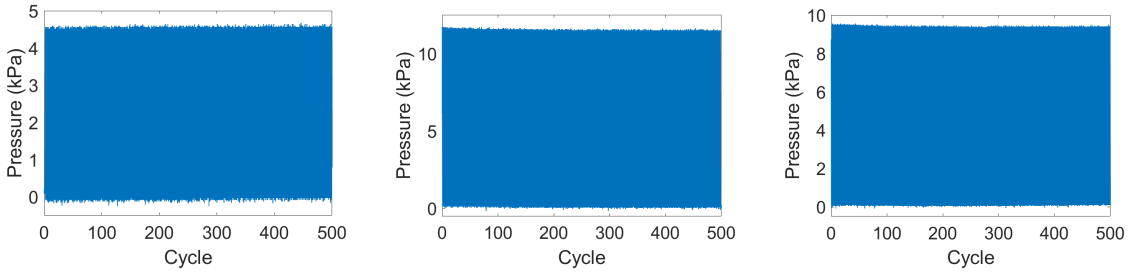

(a) S2 (b) E1 (c) S1

Figure 3.16: Durability over 500 cycles

4

System Integration

4.1 Proposed Layout

Following the characterisation process and the selection of the most suitable PSC for the application, a comprehensive schematic layout was devised and thoroughly discussed. Through careful analysis, it was determined that embedding 19 S1 PSCs around a cylinder with a diameter of 70 mm and a height of 130 mm achieves a balance between resolution and covered area. In Figure 4.1, a schematic of the final prototype and the map of the sensor distribution in the right and left hand are presented.

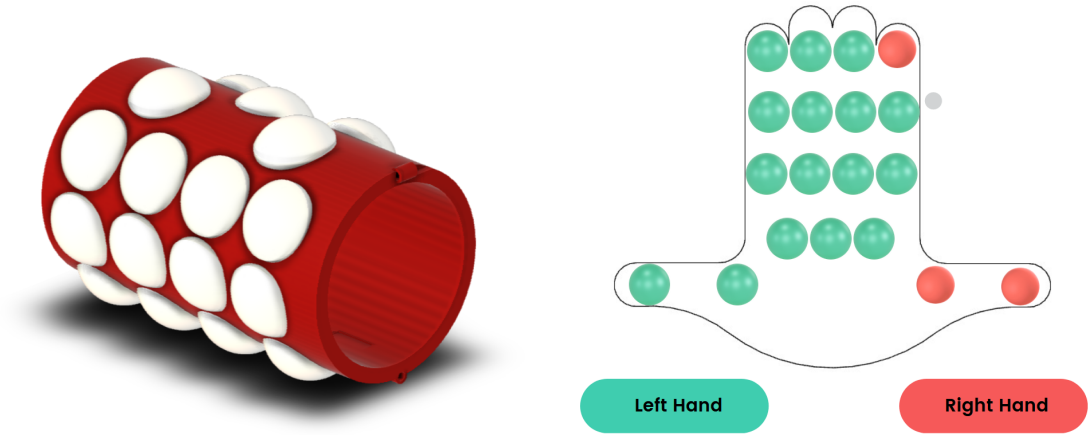

(a) (b)

Figure 4.1: Schematic of the prototype with 19 embedded PSCs (a) Cylinder and (b) Hand map: left hand in green PSC and right hand in extra pink PSCs

4.2 Calibration Procedures

4.2.1 Methodology

In order to enable the connection between the PSC and the transducer without any interference from the sensor's structure, a small plastic tube is employed. This ensures that the force applied is not influenced by the sensor. However, due to variations in the

size and placement of the tube, there exists an inner volume discrepancy among each PSC. Consequently, individual testing of each PSC was conducted to examine its force behavior at different output pressures to mitigate the risk of erroneous readings.

Displacement tests were performed at 0.5, 1, 1.5, and 2 mm, with each position being maintained for 10 seconds to attain a steady state pressure value. This calibration process was done to obtain reliable results.

In addition to the previously conducted tests, Stability Over Time tests were performed on each PSC to verify their airtightness. These tests involved applying a 1Kg weight to the sensors for a duration of 5 minutes. It is worth noting that, based on previous tests, it had been consistently observed that airtightness was confirmed within this 5-minute period. Therefore, this duration was deemed sufficient to validate the airtightness of the PSCs in the current evaluation. These measures were of utmost importance to prevent any potential misinterpretation of results.

4.2.2 Sensors Calibration Curves

To demonstrate the stability and effectiveness of the calibration procedures, Figure 4.2 presents the results obtained from both the 5-minute stability test and the calibration force procedure. During these tests, all sensors were numbered, and any sensors that failed to meet the required criteria were excluded from further analysis. The results exhibit a consistent and linear relationship, indicating the reliability and consistency of the sensor readings.

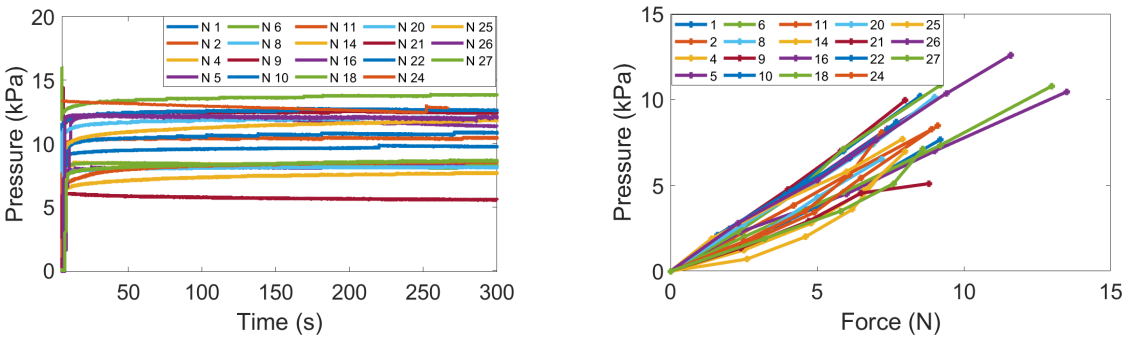

(a) (b)

Figure 4.2: Results from each PSCs (a) Stability over 5 minutes with 1 Kg weight (b) Force correspondent to output relative pressure for each PSC

4.3 Overview of the System Architecture

In order to achieve a compact design and reduce the number of analog inputs in Arduino, two CD4051BE Multiplexers (MUX), with 8 input channels each, were employed. These multiplexers transmit the analog signals from 16 sensors to the Arduino board, utilizing only two analog inputs, 0 and 1. The last three sensors left were directly connected to the Arduino using the analog ports 2, 3 and 4. Additionally, a yellow calibration

button was integrated to simplify the process of zeroing each sensor before commencing measurements. This calibration step is essential due to the fact that these pressure sensors measure relative pressure with respect to the atmosphere. Consequently, slight variations can occur between different testing experiments. Figure 4.3 shows the prototype developed.

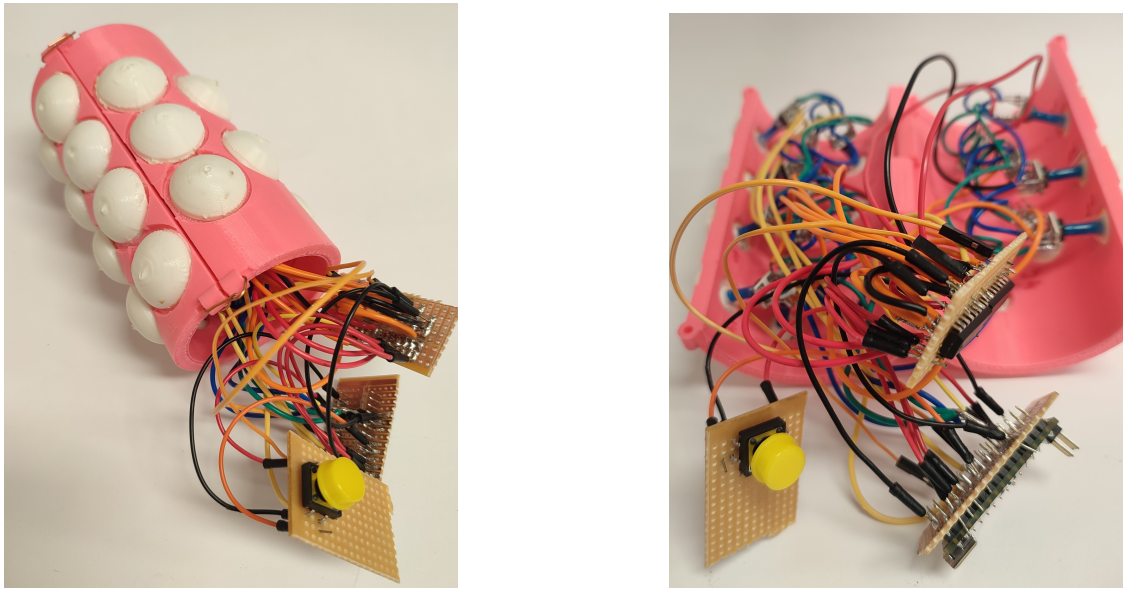

Figure 4.3: Sensorised Cylinder

4.4 Communication and Software development

Upon establishing the link between the object and the Arduino, a USB connection was employed. Subsequently, a LabVIEW "VISA Configure Serial Port" setup was established at a baud rate of 115200 to ensure fast data transmission. The data from each channel of the MUX was extracted using a while loop. These values were then stored in local variables labeled from "Channel 0" to "Channel 19". To calibrate each sensor, the corresponding force values obtained for each specific PSC in subsection 4.2.2 were correlated using a interpolation and stored in new local variables named from "Force 0" to "Force 19".

After calibration, a vector sum was performed for each finger, as represented in Figure 4.4. In (a), the purple vectors correspond to the individual forces measured by each PSC. The blue planes correspond to the fixed sections of each sensor, and the origin axis is indicated by the black arrows at the center. In (b), there is an orange vector "F" that depicts the cumulative orthogonal force magnitude corresponding to each finger force and its correspondent angle γ.

Drawing from fundamental trigonometry principles [43], Equations 4.1 and 4.2 present the decomposition of each sensor force vector, represented in Figure 4.4 in purple vectors, into its X and Y components relative to the central axis. The angle θ is obtained from the planes where the PSCs are fixed. Here, i corresponds to each sensor, ranging from 0 to 19.

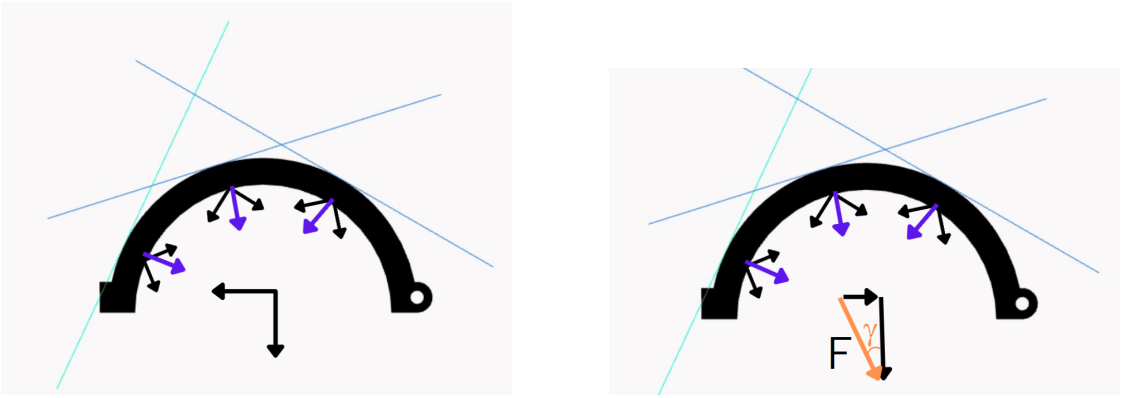

(a) (b)

Figure 4.4: Vector sum finger force

$$X = \sin(\theta) \text{ x Force [i]} \tag{4.1}$$

$$Y = \cos(\theta) \text{ x Force [i]} \tag{4.2}$$

The X and Y components from each of the three sensors on each finger (fingers 2-5) were summed to obtain the final cumulative force vector "F" for each finger. Finger force measurements were then stored in new local variables labeled as "Finger 1", "Finger 2", "Finger 3" and "Finger 4".

The force vectors of the sensors where the thumbs fit are in different planes. However, because the purpose of these calculations is to determine the grasping force corresponding to the center of the cylinder, the vectors were projected onto the same plane and then summed, using the previous approach. This sum was then stored in two local variables named "Left Thumb" and "Right Thumb".

An additional local variable named "Palm" represented the cumulative value of the last three sensors.

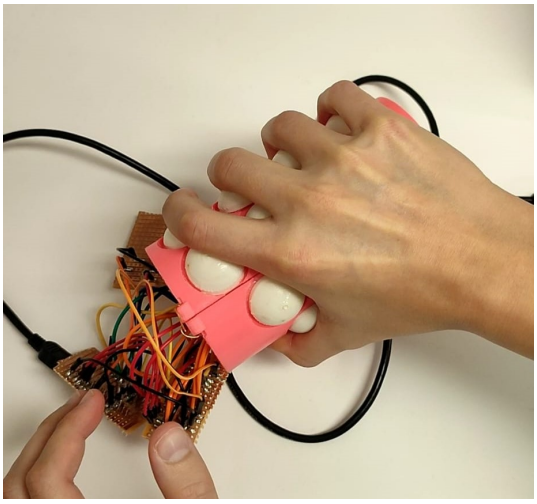

Figure 4.5: Using the Sensorised Object

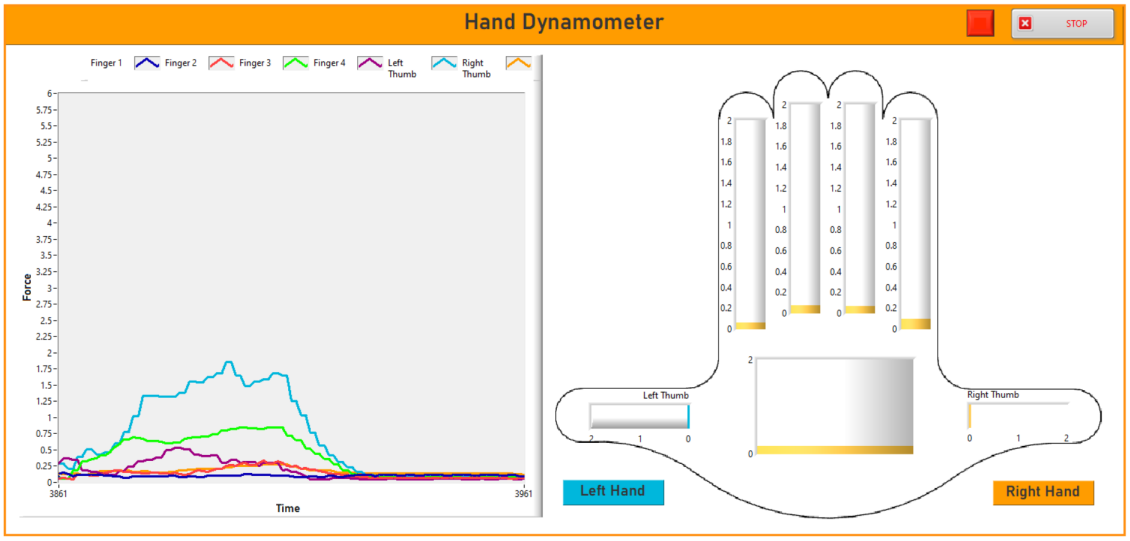

Figure 4.6: LabVIEW interface

This approach improved visual comprehension of finger forces and intensities while optimising communication speed by reducing the number of real-time display variables. Figure 4.5 illustrates the proper usage of the object.

In Figure 4.6, the LabVIEW interface is depicted, featuring a graph and a hand mapping. The hand map is categorised into "Left Hand" and "Right Hand," as all sensors are utilised in both hands except the Thumb sensors. The "Tank" level of each finger incrementally rises alongside its corresponding finger force, providing a visual elucidation of the unique contributions of each finger to the grasping force. Simultaneously, the graph on the left-hand side presents the force in real time, clearly showing which fingers are more developed in terms of strength.

Upon program initiation, an automatic window prompts the user to name an .xls file with the patient's name, which records sensor data over time, with a sampling rate of 2 Hz. The red square button located in the upper right corner of the software serves to stop recording whenever the therapist deems necessary.

For additional information concerning the LabVIEW code, refer to Appendix A, where block diagrams detailing both data acquisition and sensor calibration are presented in Figure A.1.

Additionally, Figure A.2 illustrates the calculations related to each finger's force contributions, and Figure A.3 presents the block diagram responsible for saving sensor data.

5

Conclusions and Future Work

5.1 Conclusion

In this study, several PSCs were designed, manufactured, and characterised using FEA and mechanical tests. The results showed that all designed PSCs performed well, demonstrating good stability, repeatability, negligible hysteresis, and durability, making them reliable and accurate.

Shape S2 exhibited lower sensitivity compared to the other two, as it required greater pressure changes for the same displacement or force. Shape E1 displayed improved sensitivity, but it had the drawback of producing different output pressure values when touched in various places on its surface. This reduced sensitivity around its edges, resulting in a higher force requirement for the same output pressure. Shape S1 showed the highest sensitivity and a uniformly curved surface, eliminating the edge sensitivity issue, highlighting its superiority among the others. After evaluating the results, shape S1 was deemed the most favorable design and was selected to be pursued in the next stage of the project.

Following complete characterisation, multiple S1 PSCs were 3D-printed and calibrated before implementation in the final cylinder, demonstrating crucial attributes of stability over time and linearity. The electronic system was then connected and incorporated into a small and compact design, allowing for more durable hardware and ease of use. The communication interface with the software was successfully established, showcasing independent finger force in real-time with seamless data transmission.

In this project, a prototype was completely developed from scratch, demonstrating a proof of concept. The sensorised object was capable of measuring grasping force in terms of intensity and distribution in real-time, and the data could be downloaded for further analysis, which were the main goals of this work.

5.2 Future Work

To enhance the accuracy and robustness of this system, several improvements could be implemented.

- In this study, FEM simulation did not account for pneumatic pressure in the air cavity due to the complexity associated with ANSYS Workbench's static structural analysis. The Abaqus software has the capability to model the fluid-filled air cavity and simulate the resistance that pressure applies to the walls of the PSCs. This approach could yield more accurate FEA results, aligning them closer to experimental outcomes and offering a more straightforward modulation. Additionally, some FEA simulations yielded force reaction values different from reality, a discrepancy that could be mitigated by conducting material property tests on the "Ninja Flex" part used and updating this information in ANSYS's "Engineering Library".
- Regarding the manufacturing process, exploring various 3D-printing techniques and materials could enhance printing quality and flexibility. For example, utilizing Multi-Jet Fusion with a more flexible silicone or experimenting with smaller volumes may result in greater sensitivity. A more detailed examination of 3D-printing parameters could address specific section requirements by adjusting key factors. For instance, reducing the number of layers on most of the PSC's surface while improving filament quality and quantity on the top spherical surface could increase sensitivity on the sensor's side, while still maintaining integrity and preventing gaps and air leakage.
- A notable challenge encountered in this project pertained to preventing air leakage during the assembly of the PSC with the pressure sensor. Potential solutions encompass raising the bottom height of the PSCs, though this would significantly increase 3D-printing time and resource usage. Alternatively, employing smaller pressure sensors with flat heads that do not interfere with the internal space of the PSC could address the issue.
- During the calibration process, it is important to acknowledge that tests were conducted with perpendicular plane displacements, which might not precisely replicate the complex morphology of the human body's contact areas for each phalanx. While substantial efforts were made to ensure accuracy and precision, a more intricate calibration test that accounts for the actual grasping approach and contact areas could potentially yield even more precise force measurements.
- During the calibration process, it is important to acknowledge that tests were conducted with perpendicular plane displacements, which might not precisely replicate the complex morphology of the human body's contact areas for each phalanx. While substantial efforts were made to ensure accuracy and precision, a more intricate calibration test that accounts for the actual grasping approach and contact areas could potentially yield even more precise force measurements.

- Moreover, adopting a different software platform, such as Python, holds the potential to significantly enhance the system's display speed and overall visual appeal. In the future, there is a strong incentive to conduct additional tests involving subjects within a rehabilitation period, as these tests hold the potential to yield valuable insights

In conclusion, the research conducted in this thesis has culminated in the creation of a sensor-enhanced object designed to assess both grasping force and its distribution, effectively addressing previously identified limitations. With promising prospects for further system enhancements, the future undoubtedly holds the potential to amplify the accuracy, robustness, and applicability of this tool within the domain of stroke rehabilitation, ultimately augmenting the procedures and outcomes for patients.

Bibliography

[1] J. M. Lourenço, *The NOVAthesis Template User's Manual*, NOVA University Lisbon, 2021. [Online]. Available: `https://github.com/joaomlourenco/novathesis/raw/main/template.pdf`.

[2] R. Lozano, M. N. K. Foreman, S. Lim, *et al.*, "Global and regional mortality from 235 causes of death for 20 age groups in 1990 and 2010: A systematic analysis for the global burden of disease study 2010," *The Lancet*, vol. 380, pp. 2095–2128, 9859 2012-12.

[3] "Disability-adjusted life years (dalys) for 291 diseases and injuries in 21 regions, 1990-2010: A systematic analysis for the global burden of disease study 2010," *Lancet (London, England)*, vol. 380, pp. 2197–2223, 9859 2012-12.

[4] P. Langhorne, J. Bernhardt, and G. Kwakkel, "Stroke rehabilitation," *Lancet (London, England)*, vol. 377, pp. 1693–1702, 9778 2011.

[5] "Global and regional burden of stroke during 1990-2010: Findings from the global burden of disease study 2010," *The Lancet*, vol. 383, pp. 245–255, 9913 2014, ISSN: 1474547X.

[6] M. Gittins, D. Lugo-Palacios, A. Vail, *et al.*, "Stroke impairment categories: A new way to classify the effects of stroke based on stroke-related impairments," *Clinical Rehabilitation*, vol. 35, p. 446, 3 2021-03.

[7] M. Térémetz, F. Colle, S. Hamdoun, M. A. Maier, and P. G. Lindberg, "A novel method for the quantification of key components of manual dexterity after stroke," *Journal of Neuroengineering and Rehabilitation*, vol. 12, p. 64, 2012.

[8] J. J. Daly, J. P. McCabe, J. Holcomb, M. Monkiewicz, J. Gansen, and S. Pundik, "Long-dose intensive therapy is necessary for strong, clinically significant, upper limb functional gains and retained gains in severe/moderate chronic stroke," *Neurorehabilitation and neural repair*, vol. 33, pp. 523–537, 7 2019-07.

[9] "Global, regional, and country-specific lifetime risk of stroke, 1990–2016," *The New England Journal of Medicine*, vol. 379, p. 2429, 25 2018-12.

[10] B. Sheng, J. Zhao, Y. Zhang, S. Xie, and J. Tao, "Commercial device-based hand rehabilitation systems for stroke patients: State of the art and future prospects," *Heliyon*, vol. 9, e13588, 2023.

[11] C. Grefkes, C. Grefkes, G. R. Fink, and G. R. Fink, "Recovery from stroke: Current concepts and future perspectives," *Neurological Research and Practice*, vol. 2, pp. 1–10, 1 2020-06.

[12] F. Bressi, F. Santacaterina, L. Cricenti, *et al.*, "Robotic-assisted hand therapy with gloreha sinfonia for the improvement of hand function after pediatric stroke: A case report," *Applied Sciences*, vol. 12, p. 4206, 9 2022-04.

[13] K. E. Laver, B. Lange, S. George, J. E. Deutsch, G. Saposnik, and M. Crotty, "Virtual reality for stroke rehabilitation," *The Cochrane database of systematic reviews*, vol. 11, 11 2017-11.

[14] C. R, P. F, M. A, *et al.*, "Design strategies to improve patient motivation during robot-aided rehabilitation. journal of neuroengineering and rehabilitation," *Journal of Neuroengineering and Rehabilitation*, 2007-12.

[15] C. J. Winstein, J. Stein, R. Arena, *et al.*, "Guidelines for adult stroke rehabilitation and recovery: A guideline for healthcare professionals from the american heart association/american stroke association," *Stroke*, vol. 47, e98–e169, 6 2016-06.

[16] D. J. Gladstone, C. J. Danells, and S. E. Black, "The fugl-meyer assessment of motor recovery after stroke: A critical review of its measurement properties," *Neurorehabilitation and Neural Repair*, vol. 16, pp. 232–240, 3 2002.

[17] Q. A. Boser, M. R. Dawson, J. S. Schofield, G. Y. Dziwenko, and J. S. Hebert, "Defining the design requirements for an assistive powered hand exoskeleton: A pilot explorative interview study and case series," *Prosthetics and Orthotics International*, vol. 45, p. 161, 2 2021-04.

[18] F. Cordella, F. Taffoni, L. Raiano, *et al.*, "Design and development of a sensorized cylindrical object for grasping assessment," *Proceedings of the Annual International Conference of the IEEE Engineering in Medicine and Biology Society, EMBS*, vol. 2016-October, pp. 3366–3369, 2016-10.

[19] D. J. Lin, S. P. Finklestein, and S. C. Cramer, "New directions in treatments targeting stroke recovery," *Stroke*, vol. 49, p. 3107, 12 2018.

[20] R. Kabir, S. H. Sunny, H. U. Ahmed, and M. H. Rahman, "Micromachines hand rehabilitation devices: A comprehensive systematic review," *A Comprehensive Systematic Review. Micromachines*, vol. 13, p. 1033, 2022.

[21] C. L. Taylor and R. J. Schwarz, "The anatomy and mechanics of the human hand," *Artificial limbs*, 1955-05.

[22] E. Okwumabua, M. A. Sinkler, and B. Bordoni, "Anatomy, shoulder and upper limb, hand muscles," *StatPearls*, 2023-07.

[23] G. Rimasti. "Muscles of the thenar eminence, hypothenar eminence, and central compartment group are seen in this superficial view of the right-side anterior hand." (), [Online]. Available: https://learnmuscles.com/glossary/muscles-of-the-anterior-hand-superficial-view/.

[24] P. Lyden, "Using the national institutes of health stroke scale," *Stroke*, vol. 48, pp. 513–519, 2 2017-02.

[25] Y. E. van Kooij, A. Fink, M. W. N.-v. der Sanden, and C. M. Speksnijder, "The reliability and measurement error of protractor-based goniometry of the fingers: A systematic review," *Journal of hand therapy : official journal of the American Society of Hand Therapists*, vol. 30, pp. 457–467, 4 2017-10.

[26] "Arm function after stroke: Measurement and recovery over the first three months," *Journal of neurology, neurosurgery, and psychiatry*, vol. 50, pp. 714–719, 6 1987.

[27] "Amadeo - tyromotion." (), [Online]. Available: https://tyromotion.com/en/products/amadeo/.

[28] A. Borboni, M. Mor, and R. Faglia, "Gloreha-hand robotic rehabilitation: Design, mechanical model, and experiments," *Journal of Dynamic Systems, Measurement and Control, Transactions of the ASME*, vol. 138, 11 2016-11.

[29] "Cybergrasp — cyberglove systems llc." (), [Online]. Available: http://www.cyberglovesystems.com/cybergrasp.

[30] R. Kõiva, R. Haschke, and H. Ritter, "Development of an intelligent object for grasp and manipulation research," *IEEE 15th International Conference on Advanced Robotics: New Boundaries for Robotics, ICAR 2011*, pp. 204–210, 2011.

[31] M. A. Roa, R. Koiva, and C. Castellini, "Experimental evaluation of human grasps using a sensorized object," *Proceedings of the IEEE RAS and EMBS International Conference on Biomedical Robotics and Biomechatronics*, pp. 1662–1668, 2012.

[32] R. A. Romeo, F. Cordella, L. Zollo, *et al.*, "Development and preliminary testing of an instrumented object for force analysis during grasping," *Proceedings of the Annual International Conference of the IEEE Engineering in Medicine and Biology Society, EMBS*, pp. 6720–6723, 2015-11.

[33] Y. Hao, S. Zhang, B. Fang, F. Sun, H. Liu, and H. Li, "A review of smart materials for the boost of soft actuators, soft sensors, and robotics applications," *Chinese Journal of Mechanical Engineering (English Edition)*, vol. 35, 1 2022-12.

[34] C. Tawk, G. M. Spinks, M. I. H. Panhuis, and G. Alici, "3d printable linear soft vacuum actuators: Their modeling, performance quantification and application in soft robotic systems," *IEEE/ASME Transactions on Mechatronics*, vol. 24, pp. 2118–2129, 5 2019-10.

[35] D. Gong, R. He, J. Yu, and G. Zuo, "A pneumatic tactile sensor for co-operative robots," *Sensors (Switzerland)*, vol. 17, 11 2017-11.

[36] J. Qin, L.-J. Yin, Y.-N. Hao, *et al.*, "Flexible and stretchable capacitive sensors with different microstructures," *Advanced Materials*, vol. 33, p. 2 008 267, 34 2021-08.

[37] R. Tchantchane, H. Zhou, S. Zhang, and G. Alici, "A review of hand gesture recognition systems based on noninvasive wearable sensors," *Advanced Intelligent Systems*, 2023-07, ISSN: 2640-4567. DOI: 10.1002/AISY.202300207.

[38] J. C. Hobart, S. J. Cano, J. P. Zajicek, and A. J. Thompson, "Rating scales as outcome measures for clinical trials in neurology: Problems, solutions, and recommendations," *The Lancet. Neurology*, vol. 6, pp. 1094–1105, 12 2007.

[39] G. Gao, G. Gorjup, R. Yu, P. Jarvis, and M. Liarokapis, "Modular, accessible, sensorized objects for evaluating the grasping and manipulation capabilities of grippers and hands," *IEEE Robotics and Automation Letters*, vol. 5, pp. 6105–6112, 4 2020-10.

[40] C. Tawk, H. Zhou, E. Sariyildiz, M. I. H. Panhuis, G. M. Spinks, and G. Alici, "Design, modeling, and control of a 3d printed monolithic soft robotic finger with embedded pneumatic sensing chambers," *IEEE/ASME Transactions on Mechatronics*, vol. 26, pp. 876–887, 2 2021-04.

[41] C. Tawk, M. in het Panhuis, G. M. Spinks, and G. Alici, "Soft pneumatic sensing chambers for generic and interactive human–machine interfaces," *Advanced Intelligent Systems*, vol. 1, p. 1 900 002, 1 2019-05.

[42] E. T. Gilbert-Kawai, M. D. Wittenberg, W. (W. L. Davies, and R. Gilbert, *Essential equations for anaesthesia : key clinical concepts for the FRCA and EDA*. Cambridge University Press, 2014, p. 199.

[43] M. Kendal and K. Stacey, "Teaching trigonometry," *Vinculum*, vol. 34, pp. 4–8, 1 1997-03.

A

LabVIEW Block Diagrams

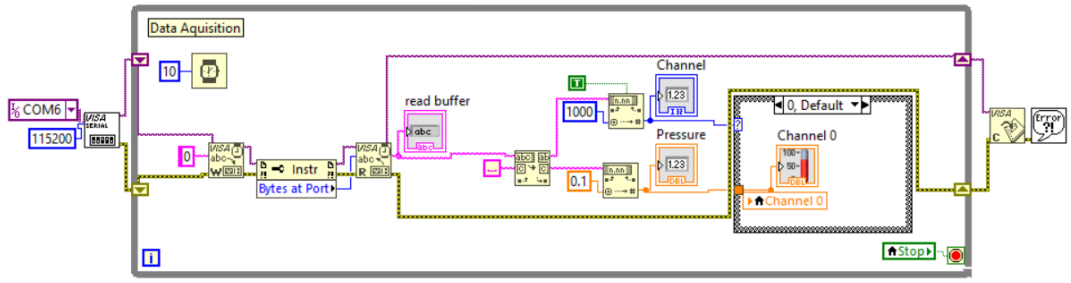

(a)

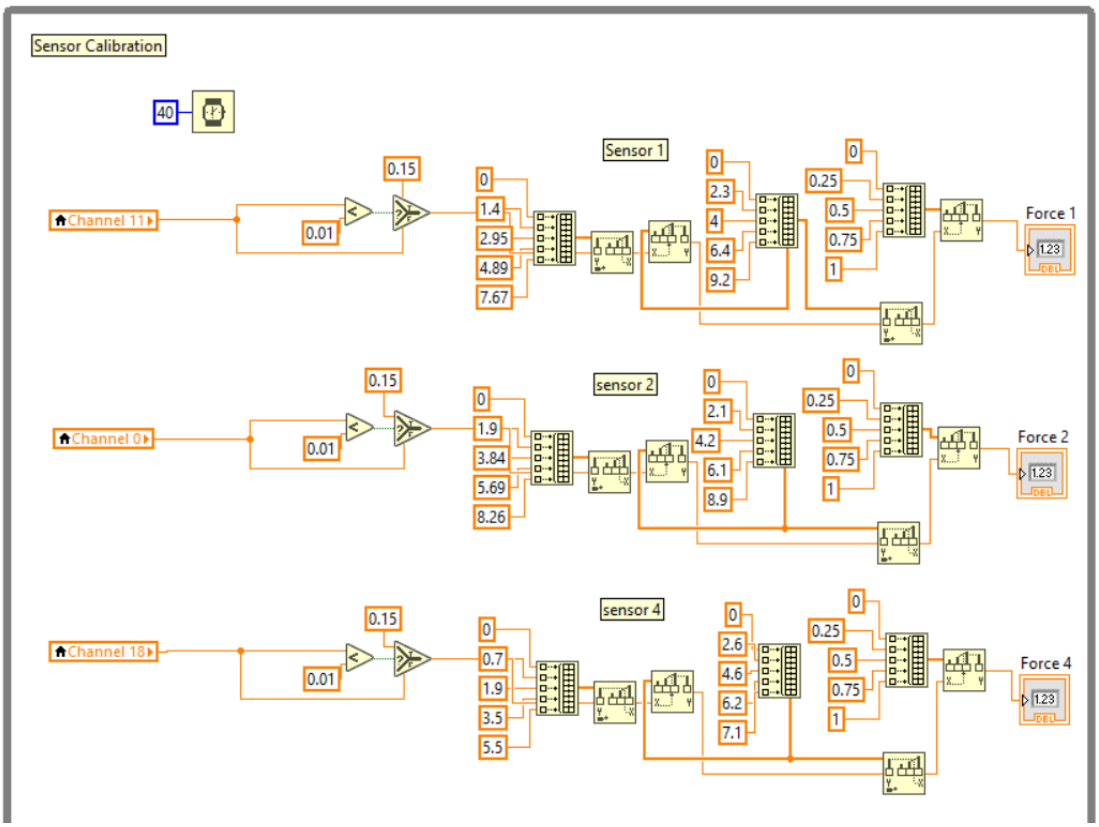

(b)

Figure A.1: LabVIEW Block Diagram of (a) data acquisition and (b) sensors calibration

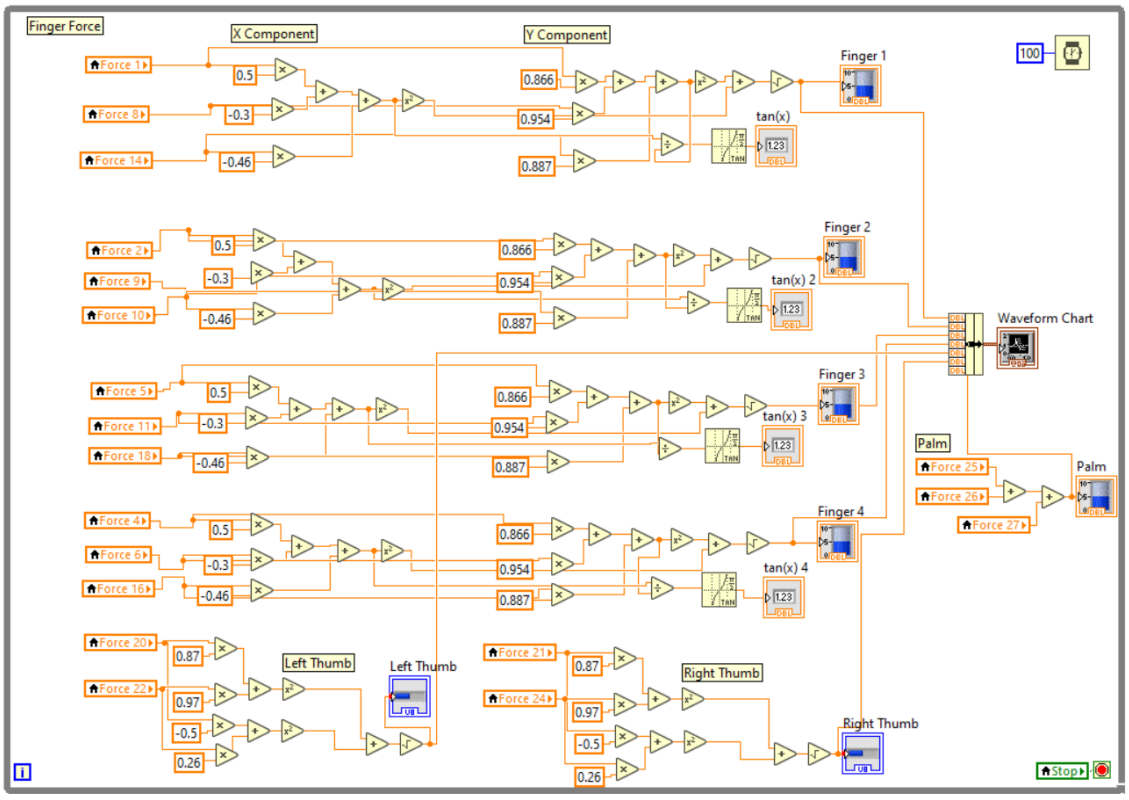

Figure A.2: Block Diagram for finger force calculations and display using LabVIEW

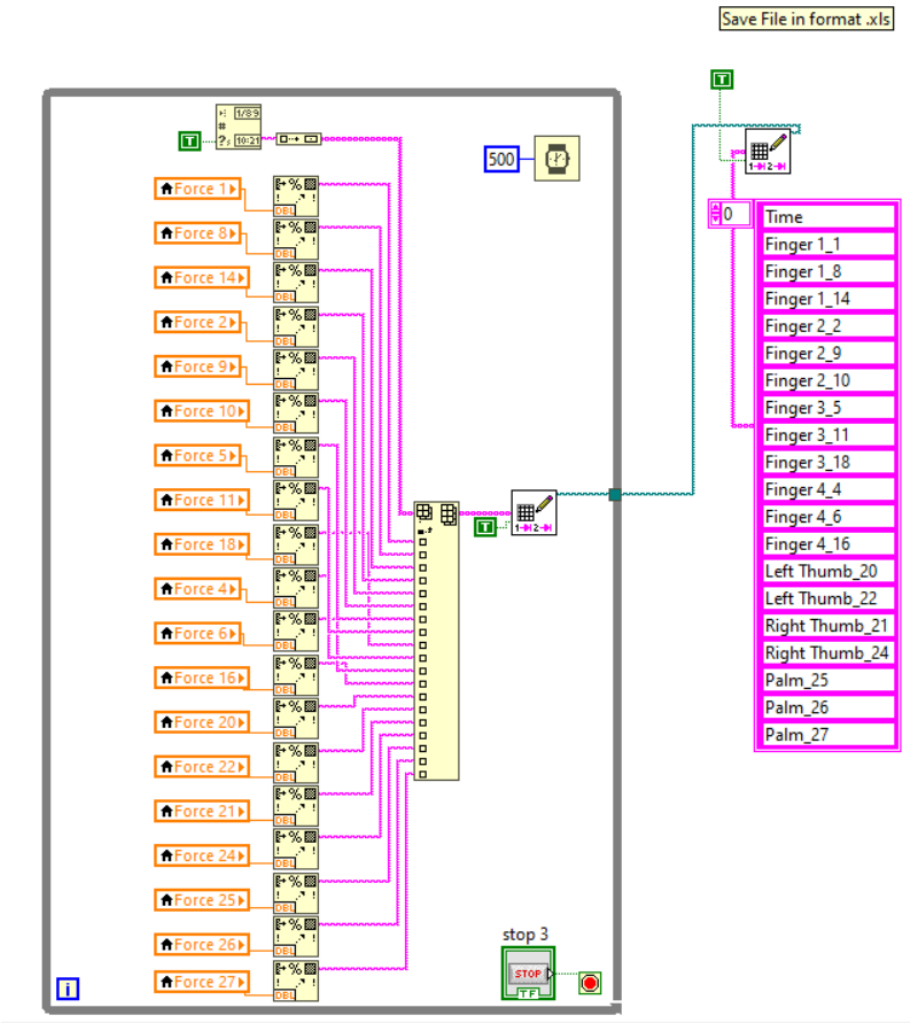

Figure A.3: Block Diagram for saving .xls file in LabVIEW